CHALMERS
UNIVERSITY OF TECHNOLOGY

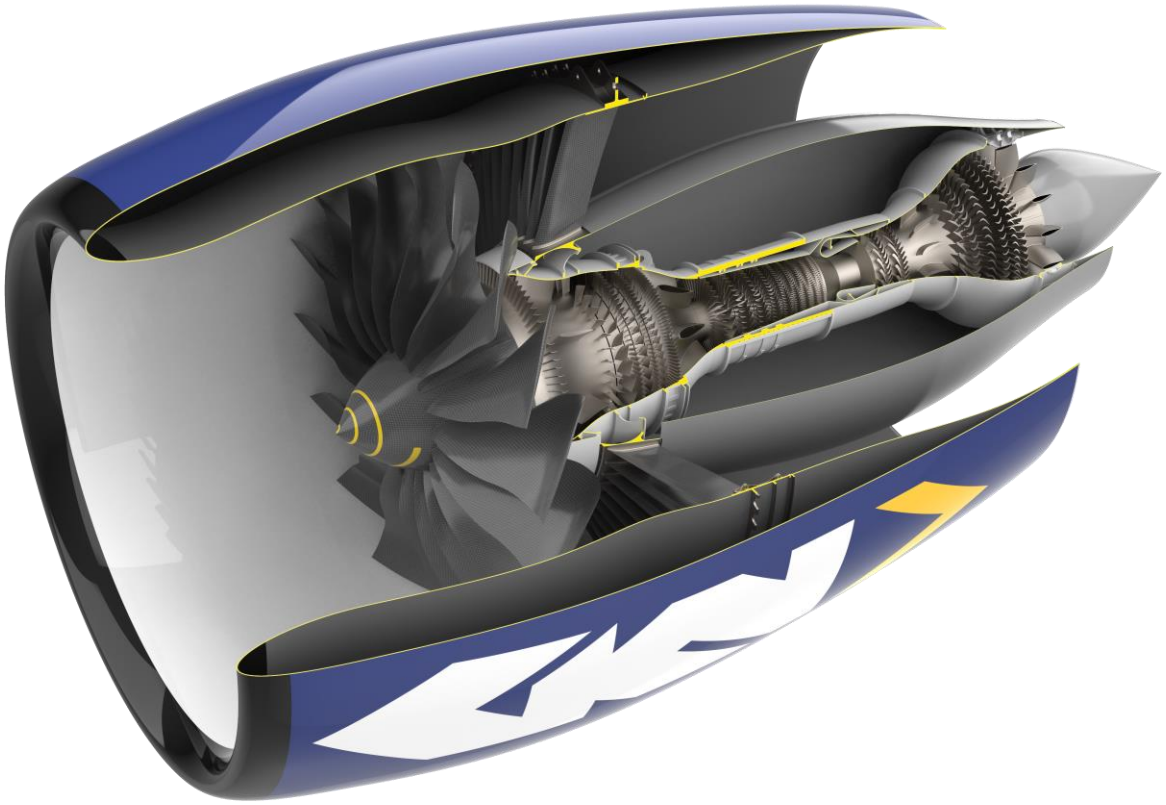

Mechanical Assessment of GKN's Outlook of Next Generation's Aircraft Engines

Master's thesis in Applied Mechanics

Martin Gustafsson

Department of Industrial and Materials Science
CHALMERS UNIVERSITY OF TECHNOLOGY
Gothenburg, Sweden 2019

Mechanical Assessment of GKN’s Outlook of Next Generation’s Aircraft Engines

MARTIN GUSTAFSSON

Master’s Thesis

Department of Industrial and Materials Science

Chalmers University of Technology

SE-412 96 Gothenburg

Sweden

Telephone +46 (0)31-772 1000

Cover:

Notional Engine - GKN’s outlook on next generation’s of aircraft engines
[Source GKN]

Abstract

Boeing New Midsize Airplane is a potential future midsize airplane that also will feature a new aero engine. GKN has conceptually designed a new aero engine based on engine performance and component design data, called the Notional Engine, and the next step is to evaluate the overall architecture from a mechanical viewpoint. This project aims to give an overview of the loads acting on an aero engine and to provide a finite element model of the Notional Engine. The finite element model will thereafter be evaluated to see how well it represents the actual engine. A general overview of the loads was obtained by studying previous whole engine mechanical models at GKN and by conducting a literature study. The finite element model was implemented into OptiStruct where maneuver load cases were simulated. A stiffness correlation study was performed at selected parts of the engine to see how well the finite element model, which consists mostly of shell elements, represents the component geometry that it builds upon. The results show that modelling with higher fidelity is needed to accurately represent the geometry that the engine builds upon. However, the results from this project can be used as a building block for future work and is a major leap forward towards accurate mechanical analyses of the Notional Engine.

Keywords: GKN; Finite element; Aero engine; Loads on an aero engine;

Acknowledgement

Firstly, I would like to thank my main supervisors at GKN, PhD Oskar Thulin and Niklas Olofsson, who gave me the opportunity to carry out such an exciting thesis project.

Secondly, I would like to thank PhD Lars Nordström and PhD Richard Avellan. You shared your expertise, were always willing to take your time to answer my questions and were a great help during my thesis project.

Thirdly, I would like to thank my examiner at Chalmers, Professor Magnus Ekh, for your support during my project.

A special thanks to my fellow thesis workers and newfound friends at GKN, you made my time at GKN a pleasure.

Lastly, I would like to show my utmost appreciation for my fiancée. Your support during my studies has been invaluable and I cannot thank you enough for that. I am sure that I would not have made it this far without you.

Abbreviations

AGB	*Accessory gearbox*
BCs	*Boundary conditions*
BNMA	*Boeing New Midsize Airplane*
CFRP	*Carbon fiber reinforced polymer*
FBO	*Fan blade off*
FCMR	*Fan case mount ring*
FEM	*Finite element model*
HCF	*High cycle fatigue*
HPC	*High-pressure compressor*
LCF	*Low cycle fatigue*
LPC	*Low-pressure compressor*
OEM	*Original equipment manufacturers*
SCF	*Structural compressor frame*
TiAl	*Titanium aluminide*
TRS	*Turbine rear structure*
WEM	*Whole engine model*

Contents

1 Introduction

An aero engine is a complex structure that contains numerous components. Therefore, it is a very large scope for a single manufacturer to develop the entire aero engine and the design of the individual components is therefore often distributed to partner companies. GKN Aerospace Engine Systems, hereinafter referred to as GKN, is such a partner company and develop structural components for aircraft engines. GKN has components installed in more than 90 % of all new civil commercial aircraft engines. This means that GKN cooperates with all the large original equipment manufacturers (OEM) i.e. General Electrics, Pratt & Whitney, Rolls Royce and Safran, which normally are responsible for the engine as a whole.

An aircraft engine is designed to withstand a large number of load cases that will or might occur during its lifetime. These loads influence the design of the structural components and the requirements are typically set by the OEMs, with the requirements for certification in mind, in an iterative process with GKN.

GKN is investing in predicting market trends to assure that they stay competitive and can grow in the future. Thus, an outlook of what is believed to be the next generation of aircraft engines, called Notional Engine, has been put forward within the company. The Notional Engine was developed to make it possible to study how design changes affect both the individual component and the entire engine system.

1.1 Background

To enable structural design of an aero engine, a whole mechanical engine model (WEM) is prepared [1]. Full system analysis is performed on the WEM, e.g. simulating the aircraft maneuvers, fan blade off events et cetera. Analysis of different load cases are performed on the WEM where critical load cases are identified for the different components. The loads result in global displacements that can be used as boundary conditions (BCs) for sub modelling of individual components [2].

The level of detail depicted is commonly quite low for the finite element model (FEM) of the WEM, and therefore, shell elements are utilized [1]. If the WEM would be modelled utilizing a much finer mesh with solid elements, it would result in too long computational time. For detailed analysis of individual components, a fine mesh of solid tetrahedron and hexahedron elements are more commonly used since these analyses often require high accuracy. The BCs for the analysis of individual components are commonly expressed in terms of forces and moments at specific locations at the component interfaces. The detailed analysis is commonly used to investigate if the individual components will sustain the loads during service, evaluating maximum stresses and fatigue life. The engine manufacturer must prove that the aero engine fulfills such demands to either the Federal Aviation Administration or the European Aviation Safety Agency.

1.2 State of the Art Aero Engines

Firstly, this section will briefly describe what a turbofan is and how it propels an airplane. This section is expanded by introducing the geared turbofan, a rather recently introduced engine architecture in the aircraft industry. Secondly, GKN's conceptual engine for midsized aircraft, called the Notional Engine, is introduced. Lastly, how the Notional Engine is mounted to the aircraft's wing is described.

1.2.1 Turbofans

Most modern aero engines for commercial airplanes are turbofans. A turbofan is a gas turbine with two fluid flows that converts the stored energy in the fuel to a thrust force that propels the airplane.

The fan, located in the front of the engine, draws air into the engine and compresses it. The air is then separated into two flows where a smaller part of the air passes through the core of the engine. The low- and the high-pressure compressor (LPC and HPC, respectively), the combustion chamber and the high- and low-pressure turbine (HPT and LPT, respectively) are all located in the core of the engine. The larger portion of the air bypasses the core, and thus, is only propelled by the fan blades. The ratio of air that bypasses the core of the engine is called bypass ratio [3].

The compressors compresses the air, i.e. raises the pressure and the temperature [4]. After the compression, the air is mixed with fuel in the combustion chamber and thereafter burnt, reaching very high temperatures. The burnt gases expand through the turbines, which powers the compressors and the fan via shafts that links them. Lastly, the gas blasts through the nozzle. The jet of gases, together with the jet produced by the flow that bypasses the engine core, produces a thrust force that moves the airplane forward [5]. A schematic view of a turbofan can be seen in Figure 1.

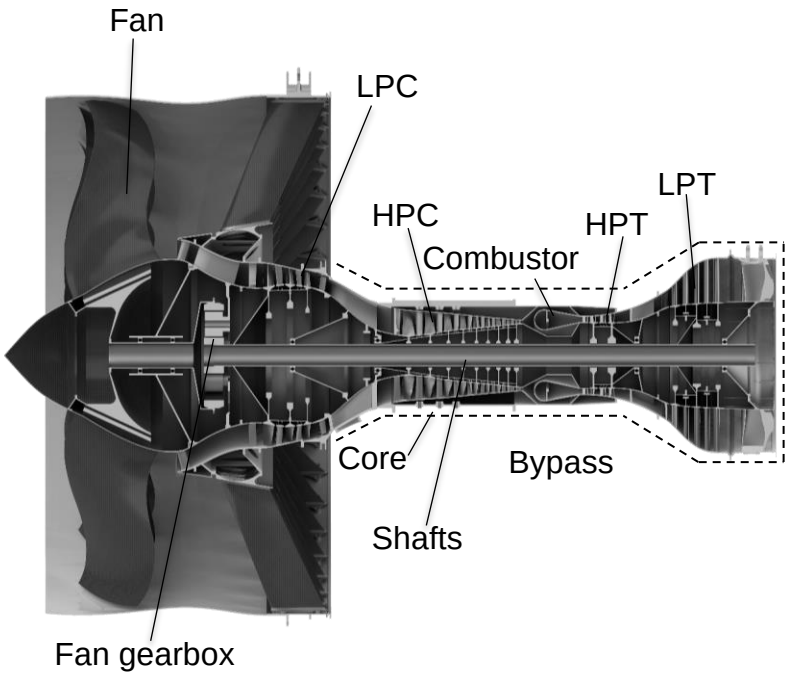

Figure 1: Schematic view of a turbofan. [Source GKN]

1.2.1.1 Geared Turbofan

In conventional turbofans, the LPT powers and is directly linked with the LPC and the fan, and the HPT powers and is directly linked with the HPC, i.e. they share shafts and thus, have the same rotational speed. In geared turbofans, a gearbox separates the shaft between the LPC and the fan. The gearbox allows the fan to have a different rotational speed than the low-pressure shaft, which allows for a more

optimal individual rotational speed for the LPC, LPT and the fan. This enables them to work more efficient. A more optimal individual rotational speed for the low-pressure shaft often results in an increased rotational speed for the LPC and LPT, which enables the LPT to expand the gas in considerably fewer stages. Fewer stages in the LPT mean that less material, and thus, a lighter LPT.

The fan jet stream, and thus, the aero engine, becomes more efficient to propel the aircraft when the differential between V_{jet} and $V_{airplane}$ goes to zero. If the airplane manufacturer gives requirements on the thrust force and the speed of the plane, parameters remaining in Equation 1 are the speed of the jet and the mass flow. To increase the mass flow, the length of the fan blades needs to increase.

A gearbox allows for a larger fan, and thus, larger mass flow, and a low-pressure shaft that rotates with a more optimal rotational speed. Due to the more efficient fan and the lighter LPT from the less constrained turbine design, the geared turbofan has potential to make the engine architecture more fuel efficient compared to the conventional turbofan, all other things being equal. The reader is referred to work by O.Thulin [6] for more about how and why larger fans make the aero engine more efficient.

1.2.2 Thrust Force

The force that makes the airplane move forward is called thrust force, F, and is generated by the aero engine. If the nozzle is unchoked, then the trust force is given by:

$$F = W(V_{jet} - V_{airplane}) \quad (1)$$

where W is the mass flow of gases through the nozzle, V_{jet} is the speed of the gases through the nozzle and $V_{airplane}$ is the flight speed of the airplane. If the nozzle is choked, i.e. the pressure ratio to the ambient air outside is beyond a critical value so that the gases cannot expand to ambient pressure, then the trust force is given by:

$$F = W\left(V_{jet} - V_{airplane}\right) + A(p_{exit} - p_{ambient}) \quad (2)$$

where A is the exit area of the nozzle, p_{exit} is the static pressure at the nozzle exit and $p_{ambient}$ is the ambient static pressure that the nozzle pressure can expand to. V_{jet} becomes fixed to Mach one, i.e. speed of sound, for turbofans with choked nozzles [4].

For the studied turbofan, there exists two flows, the flow through the core and the flow that bypasses the core. Therefore, the thrust force equations need to be adjusted. The total thrust force generated by the turbofan is thus given by:

$$F_{tot} = F_{core} + F_{bypass} \quad (3)$$

where F_{tot} is the total force generated by the aero engine, F_{core} and F_{bypass} are individually given by either Equation 1 or Equation 2, depending on whether the individual nozzle is choked.

1.2.3 State of the Art Aero Engine at GKN

This section introduces the GKN Notional Engine, a conceptual engine designed to mimic what GKN believes to be a state-of-the-art engine. The Notional Engine is designed to reflect the size, i.e. the thrust requirements, of Boeing's New Midsize Airplane, which is described in this section.

1.2.3.1 Boeing New Midsize Airplane

Boeing New Midsize Airplane (BNMA) is a potential future midsize airplane that is assumed to enter service in 2025. BNMA will probably come in two variants, one 225-seater with a flight range of 5000 nautical miles (~9260 km) and one 265-seater with a flight range of 4500 nautical miles (~8334 km) [7]. Currently, Boeing has no modern aircraft in this segment, and thus, sees a market opportunity for their new midsize airplane [8].

1.2.3.2 The GKN Notional Engine

GKN's outlook of what is believed to be the next generation of aircraft engines, called Notional Engine, is a concept engine that aims towards the size of aircraft represented by the BNMA. The Notional Engine is a geared turbofan with the most recent technologies that are mature enough to enter the market in 2025 [9]. According to GKN's estimation, the Notional Engine will generate a rated thrust force of 45 klbf (~200kN).

The estimated bare dry engine weight, hereinafter referred to as weight, of the Notional Engine is assumed to be about 15% under the baseline weight of newly developed aero engine. Weight against rated thrust force of different new aero engines can be seen in Figure 2. The baseline weight of an aero engine with a rated thrust force of 45 klbf is 3927kg, which gives an estimated weight of the Notional Engine at 3338kg. The weight reduction, compared to the baseline weight, is assumed to come from new technical innovations of components and material development.

The Notional Engine's design was derived from GKN's own engine performance models and component design data. A performance model was developed that gave a first estimation about how the aero engine would look like. The engine was then aerodynamically designed, which provided information about proper flow-path areas, number of fan-blades, et cetera. This provided input for the generation of a fully parameterized CAD-model of the Notional Engine. The CAD-model was refined based on previous experience to obtain reasonable wall thicknesses of different components, load paths through the engine et cetera [11].

The WEM of the Notional Engine makes it possible, independently of the OEMs, to estimate the overall structural behavior of the engine. The WEM allows to evaluate how changes of individual components affect the entire engine system. It also helps to build knowledge of what design changes that will lead to better overall performance. The Notional Engine makes it feasible to try out new designs of components, and thus, help to increase innovation. It also provides an opportunity to try out entire new technologies and concepts and see what potential value it can bring to the engine [11].

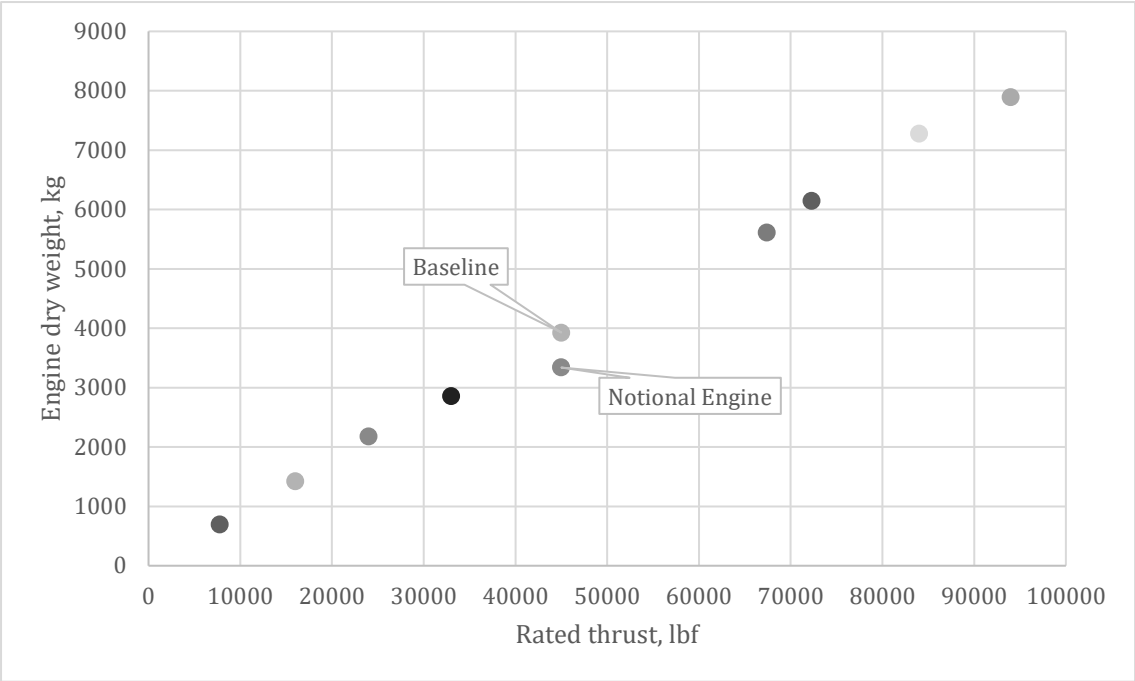

Figure 2: Weight against rated thrust force of different new aero engines. [10]

1.2.4 Attachment of Notational Engine to the Aircraft Wing

The Notional Engine is assumed to have a hybrid mounted engine to the aircraft wing. Hybrid mounted engine implies that the engine is linked to the pylon[1] via three connections. The pylon connects the engine to the aircraft wing [12].

The engine is connected to the pylon via a front mount located at the fan case mount ring (FCMR) and an aft mount located on top of the turbine rear structure (TRS[2]). The FCMR and the TRS are two of the major bearing load carrying components in the engine [12]. Two thrust links transfer the thrust force from the structural compressor frame (SCF[3]) to the aft mount. The SCF a major thrust force-carrying component [2]. This implies that the FCMR, TRS and the SCF are three major load-carrying components. A simplified version of a hybrid mounted engine can be seen in Figure 3.

[1] Other commonly used types of attachments are fan mounted and core mounted pylons.
[2] TRS is an in-house name at GKN. The TRS has different names at different OEMs. At Rolls Royce, it is called the tail bearing housing, at Pratt & Whitney the turbine exhaust case and at General Electric/CFM the turbine rear frame.
[3] SCF is an in-house name at GKN. The SCF has different names at different OEMs. At Rolls Royce, it is called the intermediate compressor case, at Pratt & Whitney the intermediate casing and at General Electric/CFM Intentional fan hub frame.

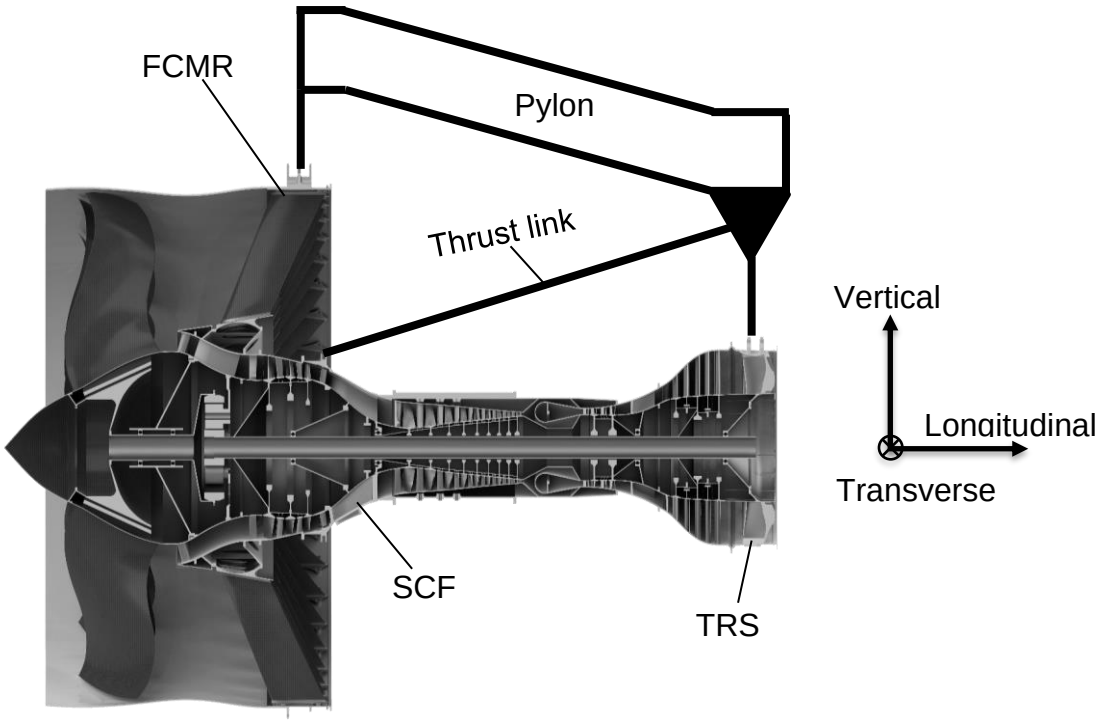

Figure 3: Simplified version a hybrid mounted engine. [Source GKN]

The mount at the FCMR have two symmetrically mirrored and angled links that fixes the engine in vertical direction. They also carry forces in the engine's transverse direction. Furthermore, together, the two links at the top of the FCMR carries moments around the engine's longitudinal- and transverse-axis. The mount at the top of the TRS has two links that are purely vertical. These links help the links at the FCMR to carry the forces in the engine's vertical direction, and together, they help to carry the moments around its longitudinal axis. Two thrust links carry the force along the longitudinal axis, e.g. the thrust force, and together, the two thrust links carry moments around the engine's vertical axis.

1.2.5 Notional Engine – Materials

The material in the Notional Engine primarily consists of titanium alloys, nickel alloys and carbon fiber reinforced polymer (CFRP). Titanium alloys have high strength to density ratio and can withstand relatively high temperatures, which makes them suitable for many components in the aero engine. Nickel alloys can withstand even higher temperatures, which makes them suitable for the hotter part in the engine. CFRP has even higher stiffness to density ratio than titanium alloys but cannot withstand as high temperatures. Thus, CFRP are being used at colder components in the aero engine. CFRP is a relatively new material for aero engines and is assumed to mainly be used for the fan section in the Notional Engine. Other materials used in the Notional Engine are titanium aluminides (TiAl) and aerospace steels. A more detailed view of the material of each component can be seen in Figure 4 and the material data, such as Young's modulus, Poisson's ratio and density, can be seen in Appendix ii.

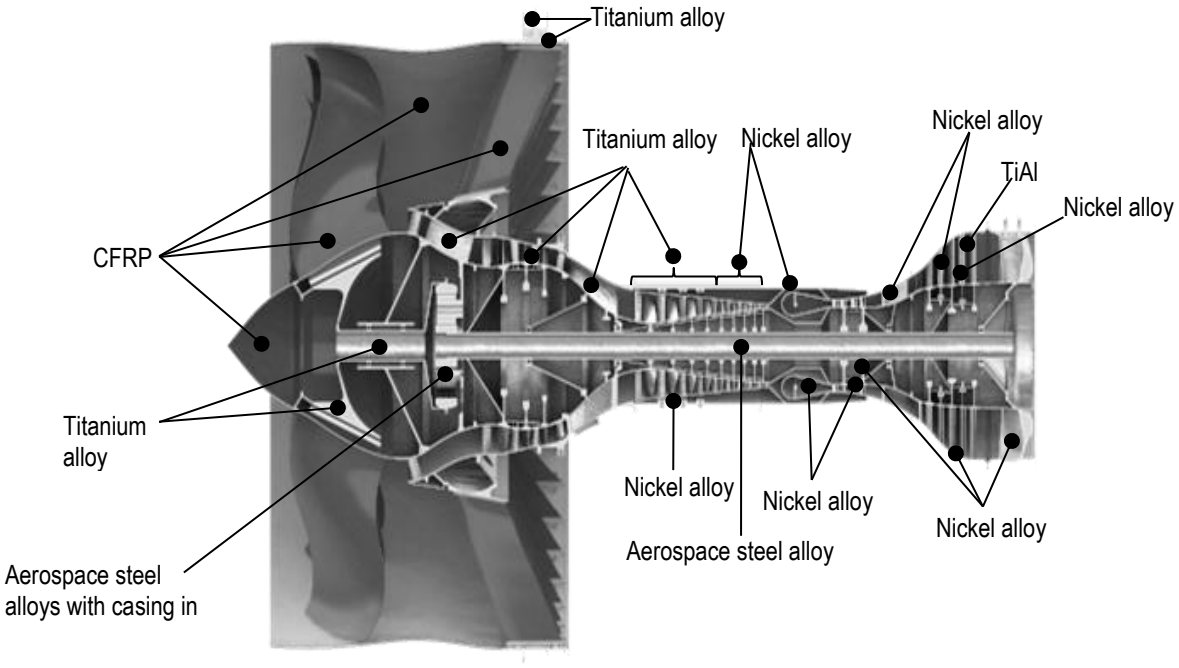

Figure 4: Materials in the Notional Engine. [Source GKN]

1.3 Whole Engine Mechanical Analysis

The mechanical design and development of an aero engine is an iterative process. A WEM, represented by a coarse meshed model of the whole engine, is prepared, for which a full engine analysis is performed. The mesh of the WEM is often represented by first order shell elements and the elements are generally quite large. Full engine analysis may include fan blade off events, climbing, cruising, turbulences et cetera.

From the full engine analysis, loads on different interfaces are transferred to a centre line load scheme, which acts as BCs to the sub-component analysis. A centre line load scheme transfers loads that act on multiple points to a point in the centre of them. For example, the loads on all nodes on the circumference of a circular flange will be transferred to the centre [2]. This results in loads on a single point instead of loads on all points on an interface. Centre line load transferring is performed to not reveal confidential information about how the different components are designed between the OEM and the designer of sub-components. For more information about centre line load transferring, see Appendix i.

From the centre line load schemes, the worst loads are identified and sub-component analyses under static condition are performed [2]. The sub-components are commonly represented by a fine meshed model of the component that most often consists of second order solid elements. Fatigue life, stress and strain criteria are often investigated during sub-component analyses.

To meet the different requirements for the components, design changes may be required, which changes the WEM and thus, the BC on the components. The updated version of the sub-component is updated in the WEM and the procedure is iterated until the component meets all the requirements. A schematic figure of the procedure can be seen in Figure 5.

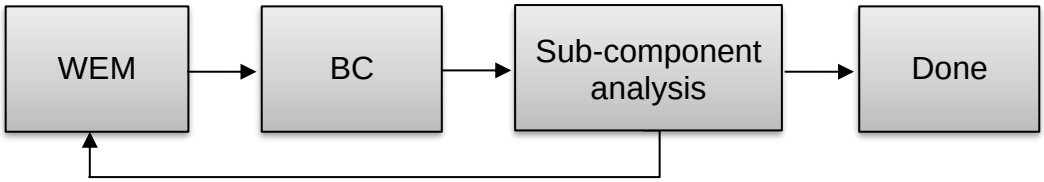

Figure 5: Schematic figure of the iterative process of the WEM.

1.4 Purpose

The purpose of this master's thesis is primarily to generate a finite element model for the WEM of the Notional Engine. This includes meshing the WEM, assigning material characteristics to each component, and applying forces and BCs to the model. Mechanical WEMs has the general purpose of generating load levels and displacements present on the interfaces between the components. For this thesis, some specific interfaces of interest are investigated with the purpose of investigating how well the notional engine WEM matches the behavior of the underlying components. Later, the WEM developed within this thesis is intended to be used to yield estimates of the mechanical requirements on the next generation's aircraft engine components. The secondary purpose of this master's thesis is to give a general overview of the external and internal loads used for WEM calculations on aero engines.

1.5 Limitations

- All components are assumed to be isothermal for modelling simplifications. This assumption is made due to the limited time of this project and has previously been made for WEM mechanical analysis at GKN with satisfactory results.
- The same assumption as for the temperature differences is also valid for the gas pressure differences between the components.
- Only a few simplified maneuver limit load cases are investigated in this thesis.
- All materials are considered to behave linear elastic, since the selected limit loads have a requirement to not cause plastic deformation.
- All calculations are simplified as linear static loading conditions, which is a common simplification for WEM mechanical analysis and has previously yielded satisfactory results at GKN.
- A sanity check, that investigates the sanity of a coarse model with a fine model, will only be performed on two of the components in the aero engine, due to the limited time of the thesis.

1.6 Disclaimer

The data published in this paper were solely to build the in-house WEM capability for the Notional Engine are not related to any characteristics of products of GKN's costumers.

2 Theory

This section aims to introduce loads that occur on an aero engine. Further, an introduction is given to the loads that the external and internal loads induce and other loads that will or might occur during an aero engine's lifespan.

2.1 Loads on an Aero Engine

An aero engine is exposed to several different kinds of mechanical loads during its lifetime. The external loads on the aero engine is caused by either the pilot when maneuvers are performed (turning, climbing, diving, landing, et cetera.), by flying in stormy weather, or when it is subjected to impacts by foreign objects like birds, hail and sand [13], [14].

The internal loads on an aero engine are caused by the thermal and pressure differences between the components, although these are disregarded in this project due to its limited time. The thrust force, which moves the airplane forward, and the centrifugal forces, caused by the rotating parts of the engine, are also part of the internal loads on the aero engine [14].

The external and internal loads are combined into load cases, which the aero engine is designed to withstand. A couple of load cases are selected with the intention to capture the critical load conditions for all the structural components in the aero engine. These load cases have been determined from tests and previous experience [13]. To get the engine certified for flight, the engine manufacturer has to prove that the engine will not fail and that it meets all required regulations that have been set up to assure that the engine will not fail critically. The Federal Aviation Administration and the European Aviation Safety Agency are the two main agencies responsible for aircraft (and thus, aero engine) certifications [15].

The mechanical loads are often grouped into limit, ultimate and fatigue loads. Limit loads are the largest loads that are likely to occur during the engine's lifespan. The aero engine must withstand such loads without causing plastic deformation of the material in the engine, i.e. the loads will not cause deterioration of engine performance or functionality. Ultimate loads are the largest loads that are likely to occur for a small batch of aero engines, i.e. will most likely not occur in all engines, but might occur on a few of all manufactured engines. The engine must not guarantee full engine performance of functionality after an ultimate load but should guarantee safe engine shut down and safe landing. Example of ultimate loads are extreme maneuver loads, loads due to blade off events, or loads coupled to failure modes.

Fatigue loads are regularly repeated loads that occur during the engine's lifespan. These loads will not cause failure directly, but the loads will cause damage to the components that may eventually cause cracks and failure of components [16]. The fatigue loads are divided into two categories, namely high cycle fatigue (HCF) and – low cycle fatigue (LCF). HCF loads are typically vibrations induced by rotational imbalances or fluctuations in air flow. These can be high frequency vibrations causing stresses below the plastic limit of the material but can still cause fatigue cracks to develop and may be critical due to the high number of cycles (more than 10^6 cycles). The LCF loads are related to regular repeating loads that occur less frequently, but has higher amplitude, compared with the HCF loads (up to 10^4 cycles). The LCF load

level in an aero engine is up to the yield limit of the different materials. Example of LCF situations are loads caused by takeoff, landing et cetera.

2.1.1 Loads Induced by the Global Loads

The external and internal loads described in the section above induce loads on the aero engine, the induced loads are described in detail below.

2.1.1.1 Rotation About a Fixed Axis

The fan, compressors and turbines all have rotating parts which rotate around their shafts, where the shafts could be considered as a fixed axis. To obtain the global loads from these rotating parts they can for simplicity be treated as rigid bodies. By choosing the coordinate frame xyz so that the z-axis follows the shafts i.e. the z-axis is the rotational axis and $\boldsymbol{\omega} = \omega \boldsymbol{e_z}$. The six equations of motions become [17]:

$$m\ddot{\bar{x}} = F_x \quad (4)$$

$$m\ddot{\bar{y}} = F_y \quad (5)$$

$$0 = F_z \quad (6)$$

$$-I_{xz}\dot{\omega} + I_{yz}\omega^2 = M_x \quad (7)$$

$$-I_{yz}\dot{\omega} + I_{xz}\omega^2 = M_y \quad (8)$$

$$-I_{zz}\dot{\omega} = M_z \quad (9)$$

where $\ddot{\bar{x}}$ and $\ddot{\bar{y}}$ is the acceleration of the centre of mass in the x and y direction respectively, m is the mass of the rotating object, ω is the scalar value of the angular velocity, $\dot{\omega}$ is the scalar value of the angular acceleration, I_{ij} is the product of inertia and I_{ii} is the moment of inertia of the rotating object.

Equations 4 to 9 are valid when the airplane cruise without maneuvers. When the airplane starts to turn, dive or climb, either the reference coordinate system (e.g. the airplane or the earth), or the coordinate system starts rotating. Which means that more aspects must be considered for calculations of the equations of motion. The reader is referred to work by A. Boström [17] for such aspects.

2.1.1.2 Gyroscopic Effects

During flight, an aero engine will be subjected to gyroscopic effects (or precession). Gyroscopic effects occur when a force is applied perpendicular to the rotational axis of a rotating object. The force will generate a torque that acts perpendicular to both the force and the rotation, visualized in the figure below [18].

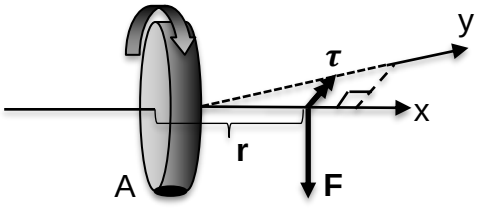

Figure 6: A force applied perpendicular to the rotational axis, which generates a torque perpendicular to both the force, and the rotational axis.

The torque vector, $\boldsymbol{\tau}$, is given by:

$$\boldsymbol{\tau} = \boldsymbol{r} \times \boldsymbol{F} \quad (10)$$

where $\boldsymbol{F}$ is the applied force vector and $\boldsymbol{r}$ is the distance vector between the mass centre of the rotating body to the applied force.

When the force $\boldsymbol{F}$ is acting on the spinning body in Figure 6, the body wants to rotate around its y-axis. To explain this a point, denoted with A, is used. Point A at the bottom of the body has a desire to move to its left due to the rotation of the body. A few instants later, the body has rotated around its rotational axis and point A has changed its position. Due to Newton's first law of motion, point A still desires to move to the left, which causes the torque [19]. The sequence is visualized in Figure 7 and Figure 8.

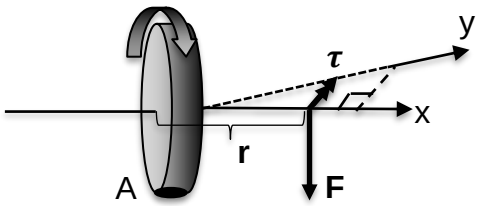

Figure 7: A force is applied perpendicular to the rotational axis. Point A desires to move to the left

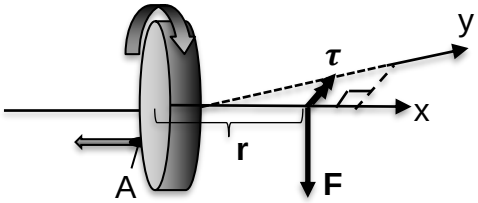

Figure 8: Point A has changed its position due to the rotation of the body. Point A still has the desire to move to the left, which generates the torque.

2.1.2 Engine Seizure

Engine seizure occurs when there is an abnormally high resistance of rotation in the rotors of the aero engine. This could occur when there is a lack of lubrication in the bearings or when the bearings are exposed to dirt. The rotating parts possesses a great amount of inertia that the engine needs to accommodate when the rotating parts lock up against the static parts [20].

2.1.3 Blade Off

Blade off events are defined as when an aero engine is losing a rotating blade, i.e. a fan blade, a compressor blade or a turbine blade. The events for the different blades are similar and such a blade off event is described in this section.

A fan blade off (FBO) event is an ultimate load case where an aero engine is losing one of its fan blades due to failure from fatigue of a fan blade, high energy impact on the fan blade, or a combination of both [21]. The detached fan blade must be contained in the engine so that it will not cause damage to the rest of the airplane. Since the FBO event is an ultimate load case, the engine should be capable of safe engine shut down and guarantee safe landing. When an FBO event occurs and the fan blade stays in the engine, it will cause loads that often are critical for design sizing of many components in the engine [21]. An FBO event can be divided into three stages – Primary impact loads, Run down imbalance and Wind milling [16]. The three stages will be described below.

2.1.3.1 Primary Impact Loads

This stage consists of the loosening of the fan blade. The fan blade causes an impact on the fan case that surrounds the fan. The impact force that the casing should withstand can be estimated according to:

$$F = m\,\omega^2\,r, \qquad 11$$

where m is the mass of the detached blade, ω is the rotational speed and r is the radius from the rotational centre to the centre of mass of the detached blade [21].

2.1.3.2 Run Down Imbalance

The sudden release of a fan blade starts the second stage. The centre of mass of the engine will move some distance from the centre of the shafts, which causes unbalance in the engine. The engine will be exposed to large reaction forces and very large vibrations due to the sudden unbalance. A safety design structure (breakage or fusing design) is common in many engines and is used to relive structural loads and tweak the load distribution so that it is more suited for the unbalanced engine. This by changing the stiffness of the rotating supports [22].

After the engine has lost its fan blade, it deaccelerates to its wind milling speed. During the deceleration, the engine might pass one or more of the engine's critical rotational speeds and might thus rotate in one of its eigenfrequencies. The loads during the run-down imbalance stage will often be quite significant due to the high amplitude of the unbalanced rotation.

2.1.3.3 Wind Milling

The wind milling stage occurs when the engine has reached steady-state, where its rotational speed is about $1/3$ of its maximum speed [22]. The engine revolves due to the aerodynamical forces that act on the fan when the airplane moves, i.e. the fan acts like a windmill. The vibrational amplitudes have been reduced to a steady state and the loads due to the imbalance are on a smaller magnitude compared to the forces in the run-down imbalance stage. However, these loads may still be severe due to the high number of load cycles and failure due to HCF is of big concern [16].

3 Softwares Used

Three software were used for the analysis of the WEM. HyperMesh was used as the pre-processor, OptiStruct as the solver of the FEM-problem and HyperView as the post-processor. These software have previously been used for studies of mechanical WEMs at GKN.

3.1 HyperMesh

HyperMesh is a multidisciplinary FEM pre-processor, developed by Altair. HyperMesh is compatible with multiple FEM-solving softwares such as Abaqus, Ansys, OptiStruct and MSC Nastran [23].

In HyperMesh, the solver-file is prepared by importing a CAD geometry and processing it before the solver-file becomes ready for the FEM solving program. HyperMesh adapt the solver-file to be compatible with the chosen FEM-solver.

3.2 OptiStruct

OptiStruct is a multidisciplinary structural analysis FEM-solver used to perform static anddynamic analysis in both the linear and nonlinear domains [24]. OptiStruct is developed by Altair and uses the solver file to create a result file for post-processing analysis.

3.3 HyperView

HyperView is a post-processing and visualization environment, developed by Altair, for FEM-analysis [25]. HyperView can be used to visualize the result file from the FEM-solver. The result could be the displacement field of a component, the stresses in a component, dynamic responses and more.

4 Generating the Whole Engine Model

This section aims to provide information about how the WEM was generated. Initially, how the mesh of the Notional Engine is generated and how the meshes of the different components are assembled is described. Thereafter, a description of how the BCs and the loads are applied to the mesh is provided. Lastly, an introduction is given of how the rotating parts and additionally required BCs were modelled.

4.1 Meshing

A performance model and a CAD model based on the performance analysis have previously been generated within GKN. CAD models for each component of the Notional Engine were imported into HyperMesh where they were meshed, i.e. the provided geometry was divided into numerous small elements. The imported CAD models mostly consists of sheets that are generated as a mid-surface from the original CAD geometry. Some simplifications of the geometry are also performed to make the meshing process of the coarse mesh smoother. The mesh primarily consists of quadrilateral shell elements since they are considered to give more accurate results when compared to triangular elements.

All meshed components were assembled into a single model. Where the interfacial nodes matched with each other, i.e. the interfacial nodes of both components had the same locations, they were merged into a single node, instead of having one node on each side of the interface. Where the interfacial nodes of the components mismatched, the interfaces were joined together with contact conditions. The contact condition FREEZE in OptiStruct was used[4]. A simplified schematic to illustrate the connection procedure between two generic components can be seen in Figure 9 and Figure 10.

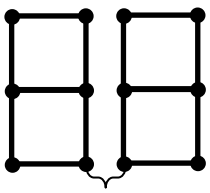

Figure 9: Nodes matches – make them share nodes at the intersection.

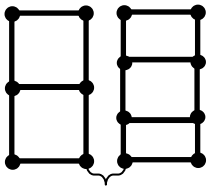

Figure 10: Nodes mismatches – use contact condition.

At the interfaces between the structural compressor frame (SCF) and the low-pressure compressor and the SCF and the high-pressure compressor, CBUSH[5] elements were used to connect the nodes between the components. The connection with CBUSH elements makes it possible to obtain the interfacial forces between the components. Note that for the connections where CBUSH elements were used, the nodes matched with each other.

[4] FREEZE implies that the surfaces are fixed together.
[5] CBUSH elements are generalized spring-damper elements where a spring stiffness could be implemented for each of the 6 degrees of freedom.
The reader is referred to the OptiStruct's user guide for more information about used elements.

The mesh consists of $\sim 400\ 000$ nodes and $\sim 383\ 000$ elements with a varying size of the shell elements between $2.4mm$, at the fan shaft, and $40mm$, at the fan case. The highest aspect ratio is 4.1 and the lowest Jacobian[6] is 0.6. Different views of the mesh can be seen in Figure 11 and Figure 12, worth mentioning is that only half of the mesh is shown in these figures.

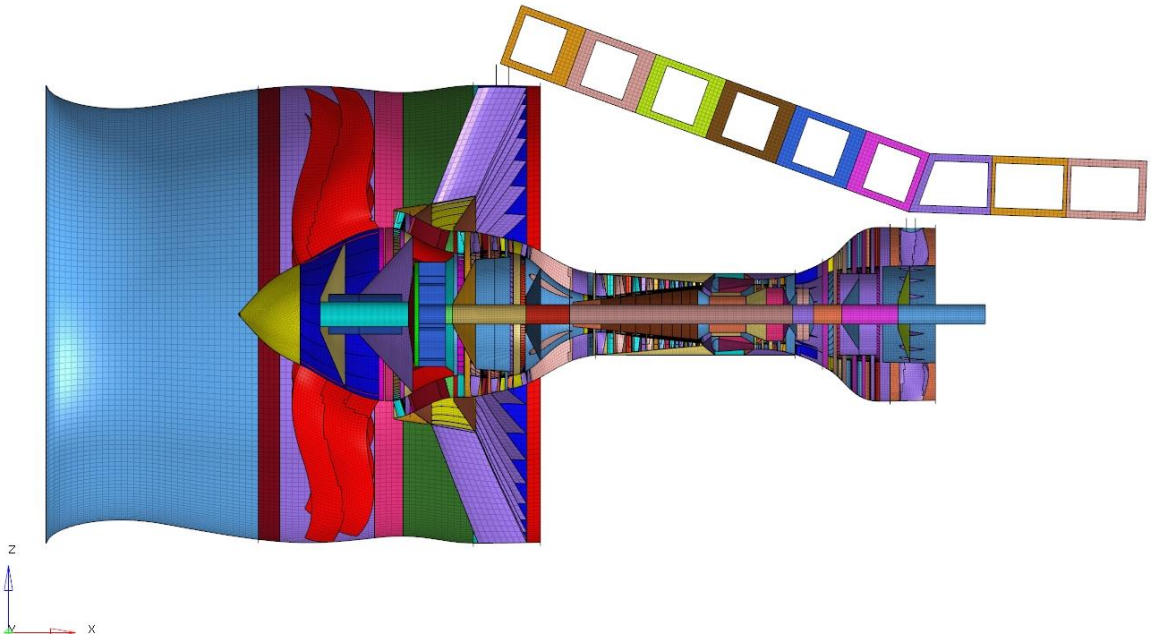

Figure 11: Part of the Notional Engine WEM mesh.

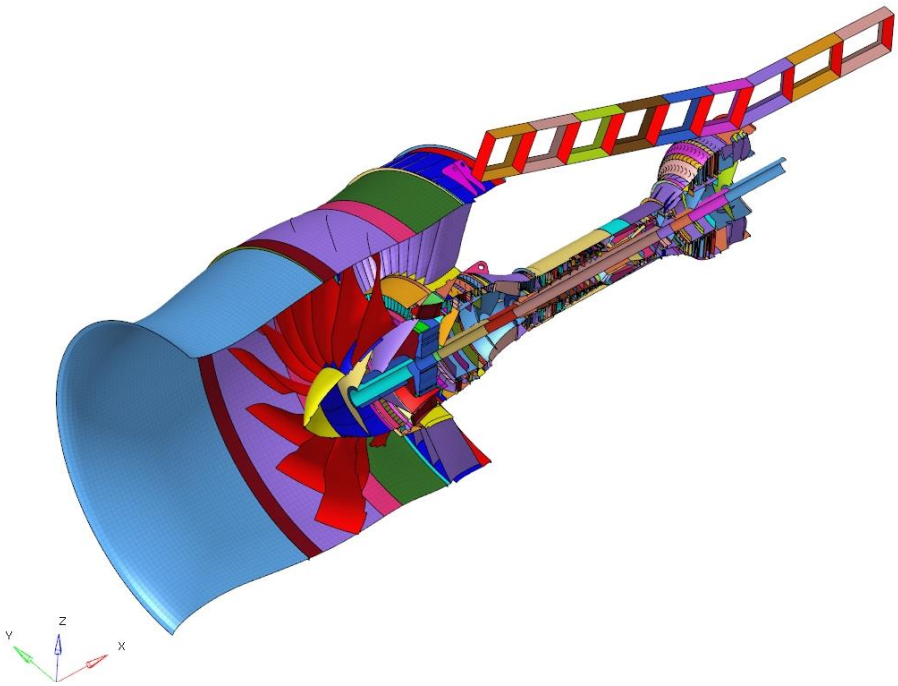

Figure 12: Part of the Notional Engine WEM mesh.

[6] The Jacobian in HyperMesh is defined as the determinant of the transformation matrix. The transformation matrix refers to the matrix used for transformation of the elements in the global coordinate system of the meshed model to the natural coordinate system used for integration.

4.2 Weight of the Meshed Notional Engine

Material characteristics according to Figure 4 and Table 5 were assigned to the meshed components. After assigning material the total weight of the WEM was $2422kg$ (not including the pylon and thrust links), which is only 74% of the estimated weight of the Notional Engine from Section 1.2.3.2. To compensate for the simplifications of the shell model and weights of components that are not included in the WEM, e.g. pipes carrying lubricates and fuel, sensors, bolts, et cetera, the density of almost all material were raised by 40%. The weights of the accessory gearbox (AGB) and the fan gearbox were set to the estimated weight of these. These assumptions gives a total weight $3291kg$ for the Notional Engine, which is just 1% lower than the estimated bare dry engine weight of the Notional Engine detailed in Section 1.2.3.2, and thus, the model is considered close enough to be representative.

4.3 Loads and Boundary Conditions

The BCs and load distribution for the Notional Engine have been inspired by the BCs and load distribution from previous experience of WEM configurations at GKN. The rear part of the pylon of Notional Engine is assumed to be fixed to the aircraft wing, which has been proven to be a valid assumption in previous WEMs at GKN. Loads on the structure induced by the thrust force and the ram drag are applied on the front bearing of all three shafts, the fan case, the rear flange of the FCMR, the HPC case and the front flange of the TRS. The torque caused by the planet gears in the planetary gearbox is evenly distributed around a selected circumferential cross-section in the fan gearbox. The value and the direction of the forces and moment are adapted for the load cases described in Section 6. A simplified version of the location of the BCs and the applied forces can be seen in Figure 13.

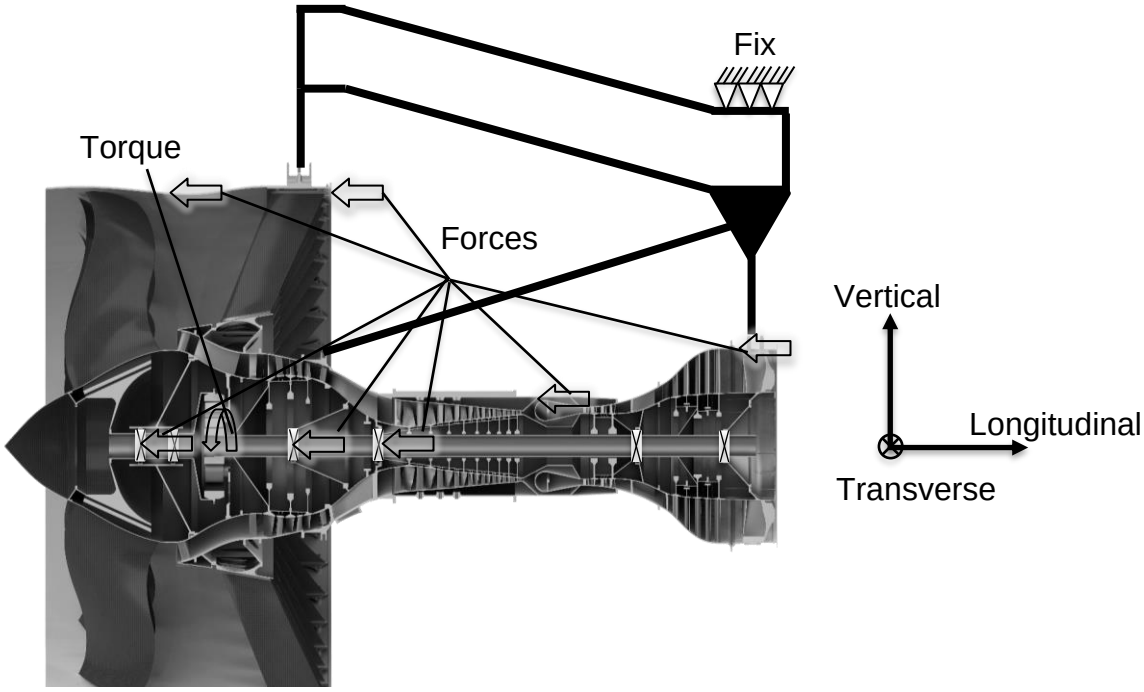

Figure 13: Location of the applied loads and boundary conditions in the Notional Engine. [Source GKN]

4.4 Discretization of Special Components

Some parts of the Notional Engine were not modeled with shell elements. The gearbox was meshed using solid tetrahedron elements, which were used to get a more accurate representation of the component. The AGB, which is located obliquely under the HPC, was modeled as a point mass with links to the HPC frame and SCF frame, which are the components the AGB is assumed to be attached to. The links to the AGB was modeled with RBE3[7] elements. Other components that were specially meshed are the engine mounts and the bearings, which are described in more detail in the following subsection.

4.4.1 Engine Mounts

The engine mounts described in Section 1.2.4 were modeled with CBAR[8] elements with a circular cross-section to represent the links between the engine and the pylon. The CBAR elements were altered to restrict them from carrying any loads in the local fourth, fifth and sixth degree of freedom[9] of one of the elements' corner nodes. The CBAR elements were also altered so that the other corner node does not carry any loads in its local fifth and sixth degree of freedom.

The constraint in the fourth degree of freedom for the first of the aforementioned corner nodes was removed to prevent the CBAR element from carrying torsion between the connection elements, which otherwise would have altered the load path in the model.

The constraint in the fifth and sixth degree of freedom were removed from all corner nodes to remove the bending stiffness of the CBAR element, making it act like a rod. The rod elements found in OptiStruct were carrying loads in its fourth degree of freedom, which is why CBAR elements were used, and thus, making the representation of the links more accurate.

4.4.2 Bearings

The position and the type of the bearings in the Notional Engine can be seen in Figure 14. The bearings in the Notional Engine were modelled with RBE2[10] elements since the bearings are considered stiff compared to the rest of the engine. The RBE2 elements connect the displacements of selected degrees of freedom, which makes them able to represent different kinds of bearings.

The tapered roller bearings and the ball bearings are assumed to be able to carry forces in the longitudinal, transverse and vertical directions and be able to carry

---

[7] RBE3 elements are elements that connects one node with one or multiple nodes. The displacement of the chosen degrees of freedom for the first node becomes the average of the displacements of the selected degrees of freedom for the connected nodes. A weighted average is also possible, where certain nodes could give more or less contribution to the displacement of the first node.
The reader is referred to the OptiStruct's user guides for more information about used elements.

[8] CBAR elements are simple beam elements where it is possible to select which degrees of freedom that the element should have.

[9] The three first degrees of freedom refers to translation along the three Cartesian axis, respectively, and degree of freedom four, five and six refers to rotation around the three Cartesian axis, respectively.

[10] RBE2 elements are rigid elements that connect one node with one or multiple nodes. The displacement of chosen degrees of freedom for the first node becomes the same as the nodes at the connected nodes.
The reader is referred to the OptiStruct's user guides for more information about used elements.

moments around the transverse and vertical axes. The roller bearings are assumed to carry forces in the transverse and vertical direction and be able to carry moments around transverse and vertical axes.

Since none of the bearings are able to carry moments around the longitudinal axis, additional BCs around the roll axis have to be added to all of the shafts to prevent rigid body motion of the shafts, and thus, making the FEM-calculations possible. The additional BCs were assigned at the centre node of a circumferential cross-section to which RBE2 elements were attached. These RBE2 elements link the assigned rotation around the longitudinal axis. The position of the additional BCs can be seen in Figure 14.

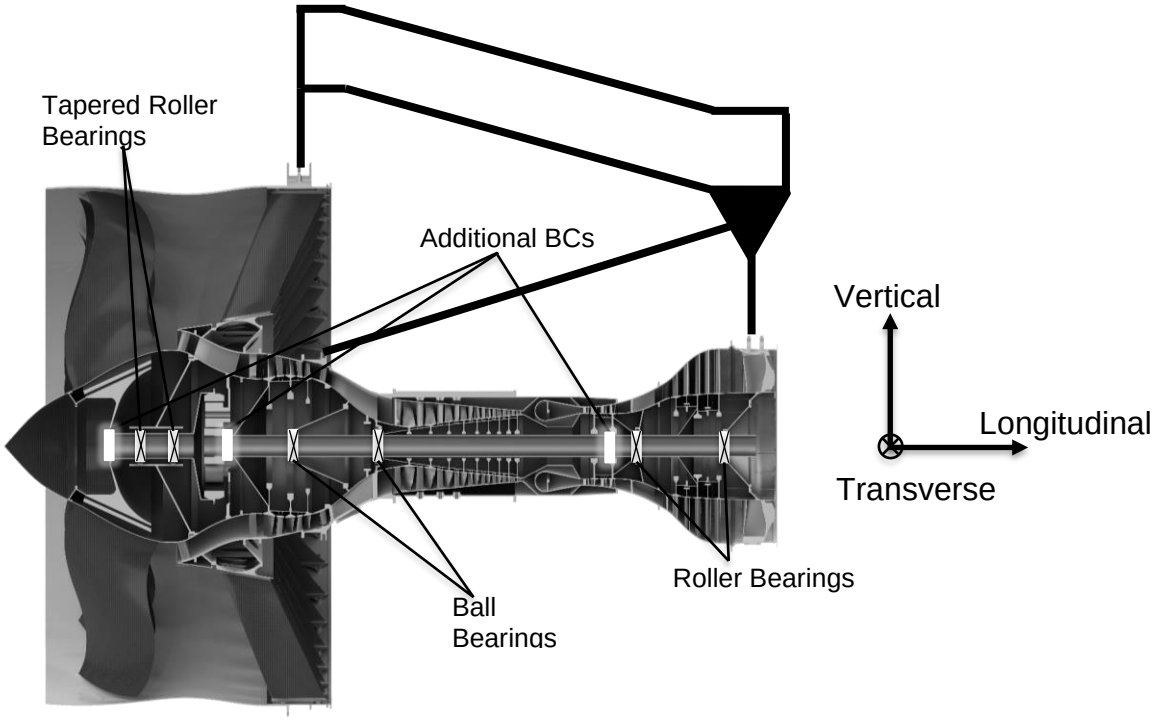

Figure 14: Bearings and additional BCs in the Notional Engine. [Source GKN]

5 Sanity Check

Each sub-component in the WEM, represented by a coarse mesh with shell elements, should have matching properties compared to a detailed model for the respective sub-component, represented by a fine mesh of solid elements [2]. This to ensure that the mechanical behavior of the true engine yields results that match whole engine tests, i.e. capture the true mechanical behavior of the engine.

To achieve a corresponding mechanical behavior for a shell model compared to a solid model a number of conditions apply [2], which all follow below. The first being the overall mass levels must match for both models. Furthermore, the stiffness and the mass moment of inertia when evaluated at the component interfaces have to match up. Moreover, the mass elements in the shell model must be also distributed in such a way that the model's basic mode shapes and eigenfrequencies match the corresponding properties for the solid model.

To investigate how well the shell model of the Notional Engine corresponds to a fine solid model a sanity check of the stiffness for two of the components were performed, similarly to the work by Raja's [2]. The selected components for the sanity check were chosen to a fan blade and the SCF. The SCF is introduced initially in this section together with the procedure of the sanity check. Thereafter, the sanity check for the fan blade is described.

5.1 Structural Compressor Frame

GKN is responsible for the design of the SCF for some of the major aero engines that are available on today's market. The SCF hosts the thrust lugs, and thus, it is essential for the load distribution in the aero engine [2]. The SCF is located between the LPC and the HPC, see Figure 1 and Figure 3. A more detailed view of the solid model of the SCF in the Notional Engine can be seen in Figure 15.

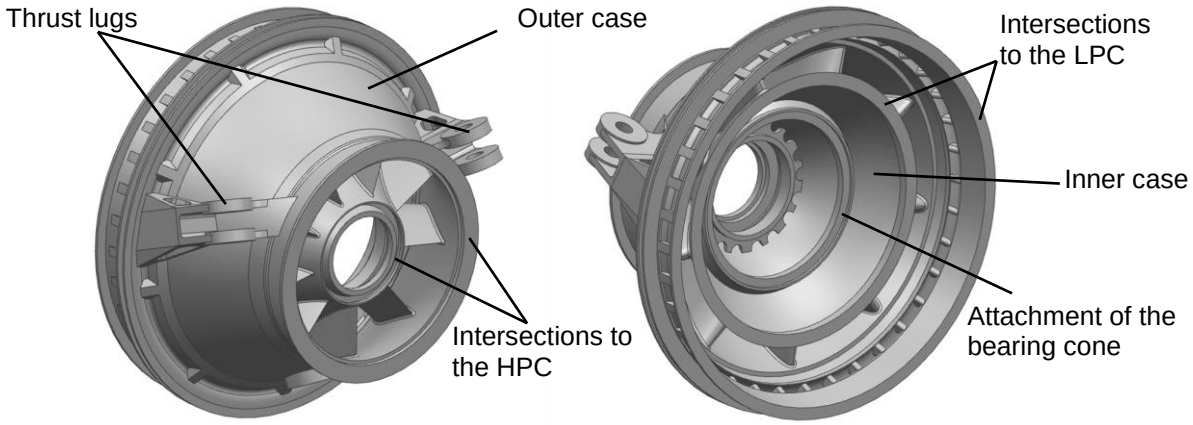

Figure 15: Solid model of the SCF in the Notional Engine. [Source GKN]

5.2 Sanity Check Structural Compressor Frame

The solid model of the SCF consists of a fine mesh with second order tetrahedron elements and the shell model is the same model as the one generated for the WEM. The mesh for the solid and the shell model can be seen in Figure 16 and Figure 17 respectively. An identical set of material properties were assigned to both the shell and the solid model, which is the same material properties as specified in the WEM.

The shell and the solid model have been assigned BCs and loads at corresponding sections of the models. It shall be noted that for the solid model, the BCs and loads were only applied at the corner nodes of the concerned elements.

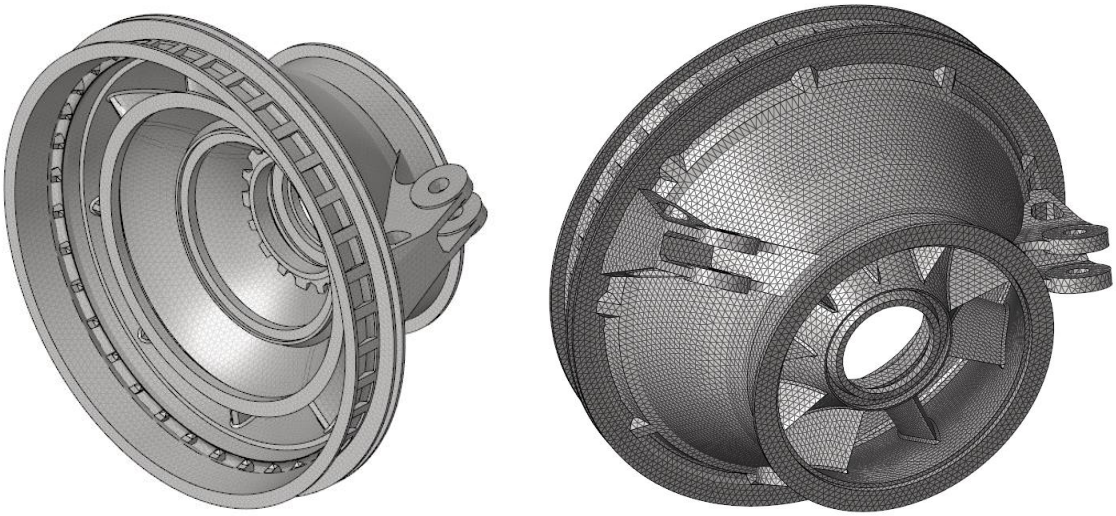

Figure 16: Solid mesh of the SCF in the National Engine.

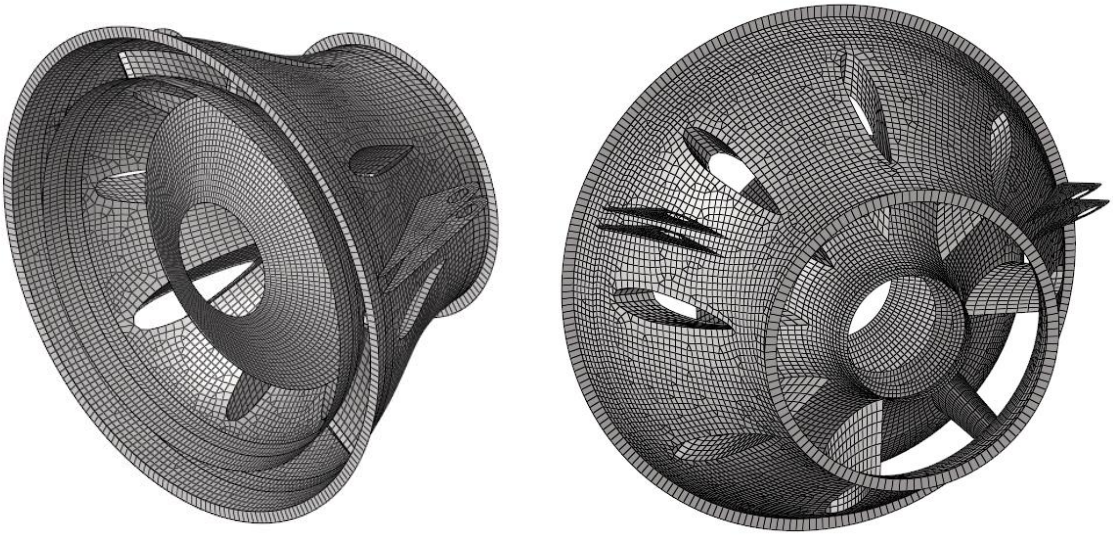

Figure 17: Shell mesh of the SCF in the National Engine.

There exist some differences between the solid model and the shell model of the SCF. The shell model is a simplified version of the solid model where details, which could have caused problems in the shell meshing process, were removed. The shell model was created as a mid-surface model of the simplified solid model, where different thicknesses were assigned to different sections of the shell model. Another difference is that both the inner and outer cases are hollow where the guide vanes attach in the shell model, but not in the solid model. This simplification was made to more accurately represent the final overall design of the Notional Engine. A bearing cone that carries the ball bearing between the SCF and the LP shaft is included in the shell model, but not in the solid model. It was attached to the shell model to simplify the meshing process. The inner connection between the SCF and the LPC also differs between the shell and solid model of the SCF. The shell model is also a little bit shorter in all directions compared to the solid model.

The SCF in the sanity check is assumed to be fixed at the outer intersection to the HPC. Loads and moments were applied at the midpoint node of one of the thrust lugs and at the centre-line node of the outer flange that connects the SCF to the LPC. At the thrust lugs, RBE2 elements were used to connect the midpoint of the thrust lugs to its circumferential nodes. RBE3 elements were used to connect the circumferential nodes to the centre-line nodes at the outer intersection. Simplified illustrations of the applied BCs and the applied loads of the solid model can be seen in Figure 18 and Figure 19.

At the three nodes described above, a force of $1000\ N$ were applied in the global X-, Y- and Z-direction respectively and a moment of $1000\ Nm$ were applied around the global X-, Y- and Z-axis respectively. All applied forces and moments were applied in separate setups, resulting in 18 different load cases, which for each a linear static analysis was performed.

The stiffness was measured as the applied load divided by the displacement of the node where the load was applied. The stiffness was measured in N/m for the cases where a force was applied and in N for the cases where a moment were applied. The global coordinate system of the SCF model can be seen in Figure 18.

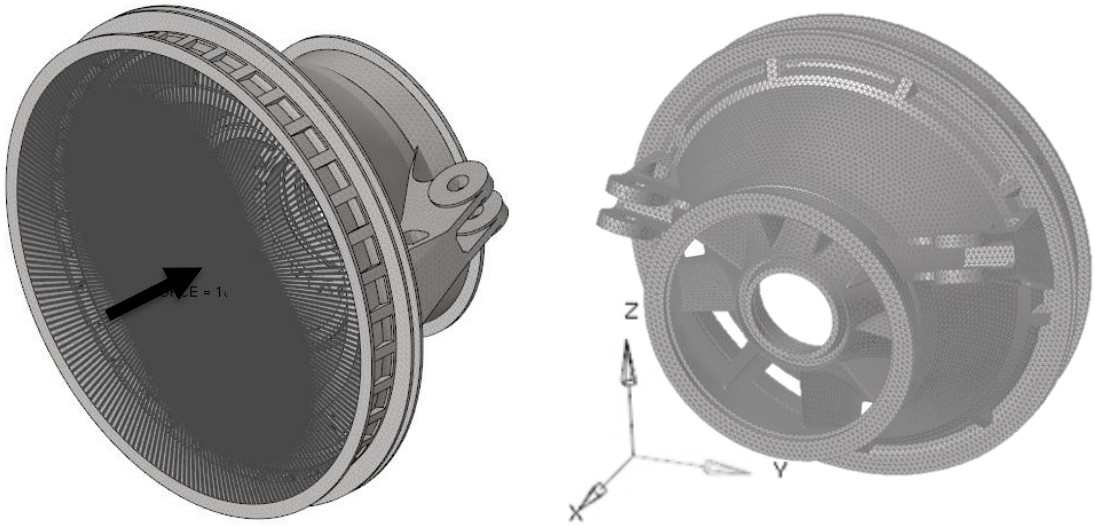

Figure 18: Left: Position of the applied load at the outer intersection at the SCF. Right: The SCF and its relation to the global coordinate system.

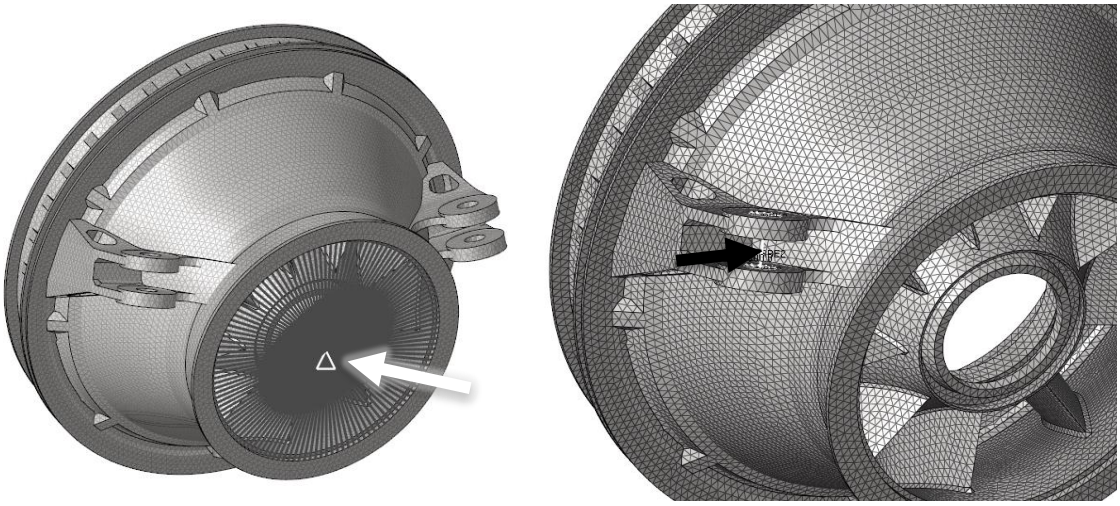

Figure 19: Left: Position of the BC for the SCF.
Right: Position of the applied load at the thrust lug at the SCF.

5.3 Sanity Check of a Fan Blade

A sanity check, similar to the sanity check of the SCF, was performed on a fan blade. The fan blade is one of many rotating parts in the aero engine, and centrifugal and gyroscopic forces for rotating parts have been excluded in previous WEMs for commercial engines at GKN. A preliminary assessment of forces due to rotating parts was performed at the WEM and gave initially questionable results, and thus, the fan blade was decided to be investigated further.

A solid mesh consisting of second order tetra elements was generated for the fan blade geometry, which can be seen in Figure 20. The shell model of the fan blade has the same mesh that is being used in the WEM and can be seen in Figure 20. The same material properties were assigned to both models, which however differs from the material specified for the fan blades in the WEM. Instead of having orthotropic material properties for CFRP material, as in the WEM, the material was changed to isotropic material properties to obtain results that are easier to compare. The isotropic material has the same Young's modulus as the titanium alloy for modelling simplification purposes, however, the density of the CRFP was kept and used for the reliability check.

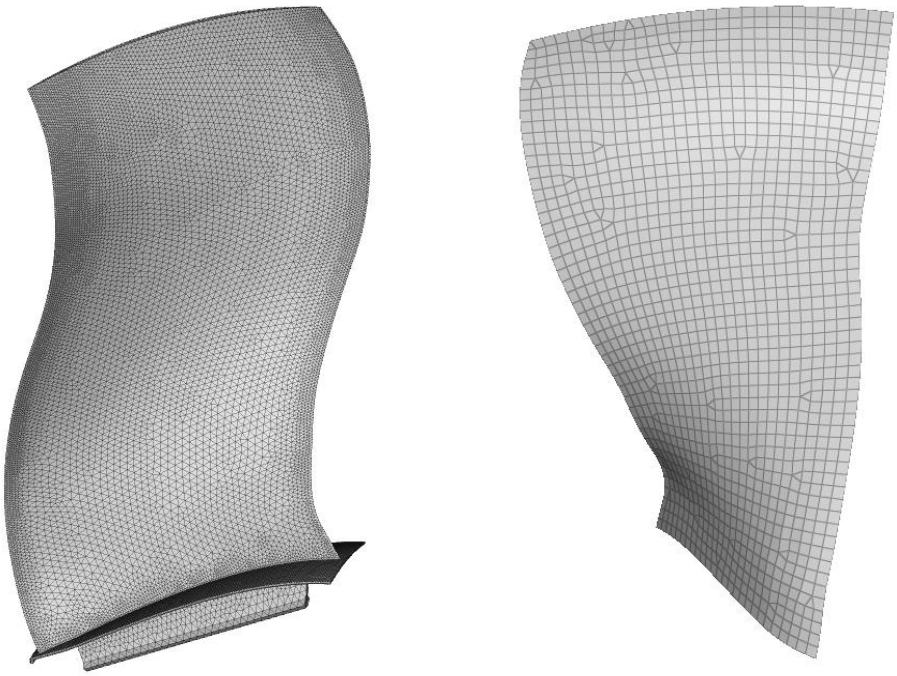

Figure 20: Left: Solid mesh of one fan blade.
Right: Shell mesh of one fan blade.

The BCs and loads were generally assigned at the same location in both the solid and the shell model of the fan.

There exist some differences between the solid model and the shell model of the fan blade. The shell model is a simplified version of the solid model where certain details were removed. The attachment to the rotation cone of the fan blade is not included in the shell model, instead, the attachment is part of the fan hub in the shell model. This was done to simplify the meshing process of the shell model. The shell model was created as a mid-surface model of the simplified shell model. The solid model has varying thickness over the blade and is thicker closer to the attachment of the rotating cone. The shell model is assumed to have constant thickness over the entire fan blade.

The fan blade in the sanity check is assumed to be fixed where it is attached to the rotating cone in the fan assembly. The fan blade is about $800mm$ long, $400mm$ wide and $9mm$ thick. The assigned BCs for both the solid and the shell meshed fan blade can be seen in Figure 21.

A static load distribution is applied to the fan blade to correspond to the centrifugal forces that the fan blade will be subjected to when it is rotating at $2500rpm$. This rotational speed represents the expected maximum rotational speed of the fan blade, and thus, yields the expected maximum displacement of the fan blade during normal engine operation. The static load generated by rotation is modelled with the load card called RFORCE[11] in OptiStruct. The RFORCE card requires a node that marks the centre of rotation, a vector that marks the axis of rotation and a coordinate system for

[11] RFORCE is a load card that represent a static loading condition due to rotations with constant angular velocity and/or angular acceleration.
The reader is referred to the OptiStruct's user guides for more information about different load cards.

the vector. The load card also requires a set of elements that it should act upon, an angular velocity and/or an angular acceleration in revolutions per unit time of the said elements [26].

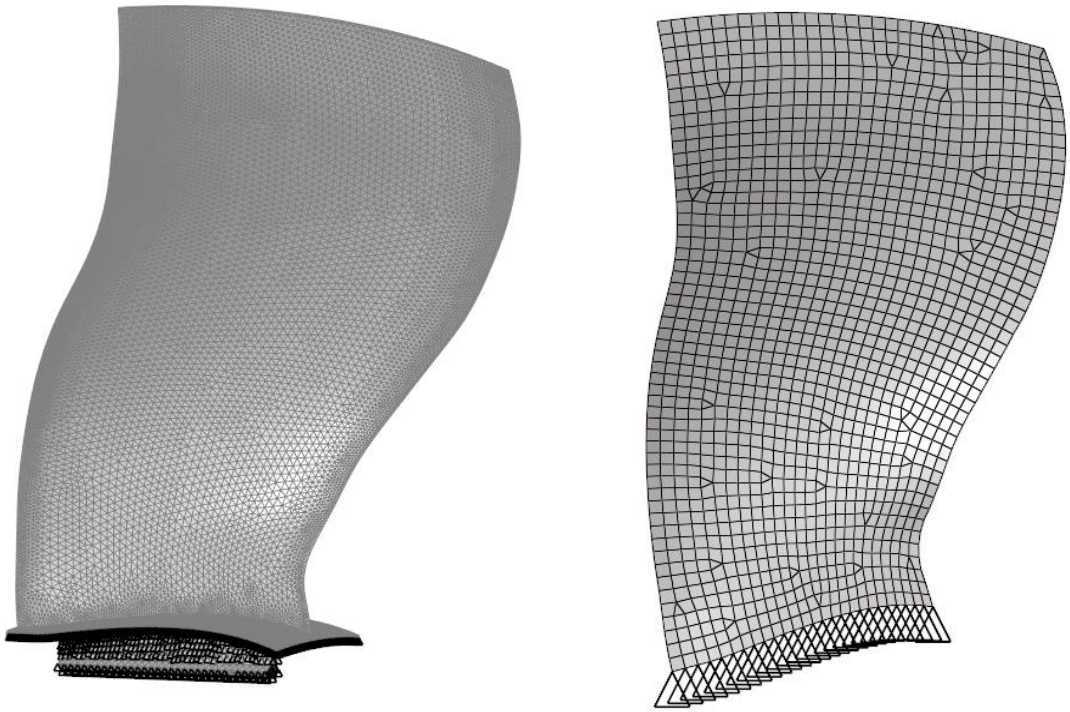

Figure 21: Left: Position of the BC applied to the solid fan blade model.
Right: Position of the BC applied to the shell fan blade model.

The node that marks the centre of rotation is selected as a node at the rotational axis of the engine's rotational parts. The selected coordinate system is the global coordinate system, which is a Cartesian coordinate system where the X-axis is the longitudinal-axis and the Z-axis is parallel to the vertical-axis. The selected axis of rotation is the X-axis and the set of elements is chosen as all the elements in the models. The implemented load card in OptiStruct format can be seen in Figure 22.

Name of the load card	Load number for implementation	Node number of rotational centre	Coordinate system number	Scalar value of rotational velocity	X-direction of rotational vector	Y-direction of rotational vector	Z-direction of rotational vector			
	0		1							

RFORCE	1	23000138	0	41.670	1	0	0			
	0		1							

Figure 22: Top: Description of the load card RFORCE card in OptiStruct.
Bottom: RFORCE load card in OptiStruct used for the sanity check of the fan blade.

To further investigate the reliability of the RFORCE load card, in a separate simulation, a force, with the magnitude of the force that occurs at the hub of the fan blade due to the rotation of a simplified blade, was applied to the top face of the fan blade and set to act in the fan blade radial direction, see Appendix iv for how the magnitude was determined. It shall be noted that this leads to overestimated

displacements for the case of a simplified blade as the static load distribution in the blade in reality gets lower with greater radius, but will, however, be handy as a reference for comparison.

The thickness of the shell meshed fan blade was also later updated from a uniform thickness of 9mm to a tapered thickness distribution along the blade that is more representative of the solid meshed fan blade, i.e. a larger thickness at the hub and thinner at the tip of the blade. The same loads and BCs as for the uniformly thick blade were also applied to the updated shell meshed fan blade with varying thickness.

A simplified blade geometry, see Figure 23, was also set up to further aid the sanity check for the fan blade. The simplified blade was assumed to have the same BCs as for the fan blade described above and was discretized as one single solid element.

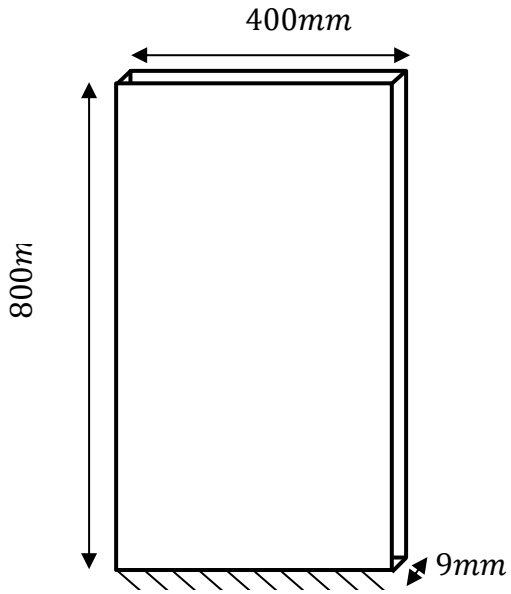

Figure 23: Simplified blade used in the sanity check evaluation of the fan blade.

6 Whole Engine Model Design Load Cases

This section introduces the selected design load cases for the WEM, what they represent and how the applied loads are distributed over the Notional Engine. Worth mentioning is that no rotation of rotational parts is modeled in the selected designed load cases, this is due to uncertainties with the implementation of such rotation, see Section 7.2 for further information about rotating parts in the WEM.

The selected design load cases simulate different situations that the aircraft most likely would be exposed to during its lifetime and represent different limit loads. Examples of such conditions are cruising with a net thrust force of $30.5kN$ with different g-forces that occur due to inertia, gusts or turning. Such loading cases have previously been analyzed for past WEMs at GKN. The selected design load cases represent the individual contributions from loads caused by the propulsion of the aircraft and loads from the accelerations the structure experience, called g-loads where g denotes the acceleration expressed in the unit of gravitational constants, and are analyzed independently from each other. The applied load distribution due to the propulsion of the aircraft can be seen in Table 1, where the applied forces have been normalized with the net thrust magnitude. The selected design load cases can be seen in Table 2.

Table 1: Load distribution Notional Engine, scaled with the net thrust magnitude.

Net Thrust	**-1**
Front bearing fan shaft	-1,45
Front bearing LP shaft	2,45
Front bearing HP shaft	-0,2
HPC Case	-3,4
Front flange TRF	0,55
Rear flange FCMR	1,05
Gearbox Torque [Nm]	70
Fan case	-3,2
Gross Thrust	-4,2

Table 2: Selected design load cases.

NUMBER	**LOAD CASES**
1	Cruise thrust (30.46kN), no g-loads
2	-3g along vertical axis
3	1.5g along pitch axis
4	-1.5g along pitch axis
5	-3g along vertical axis + 1,5g along pitch axis
6	-3g along vertical axis - 1,5g along pitch axis
7	-3g along vertical axis + Cruise thrust
8	1.5g along pitch axis + Cruise thrust
9	-1.5g along pitch axis + Cruise thrust
10	-3g along vertical axis + 1.5g along pitch axis + Cruise thrust
11	-3g along vertical axis - 1.5g along pitch axis + Cruise thrust

7 Results

The results from the sanity check and the results from the different load cases are presented in this section.

7.1 Sanity Check Structural Compressor Frame

The shell meshed SCF has a mass that is 62% of the mass of the solid meshed SCF. The measured stiffness at the rear outer flange, when keeping the front flange fixed, with initial thickness distribution can be seen in Figure 24 and an updated evaluation with a thickness increment of 40% for the inner and outer case can be seen in Figure 25. The measured stiffness at a thrust lug, when keeping the front flange fixed, can be seen in Figure 26. All evaluated stiffnesses were normalized with the stiffness of the solid model for each load case at each load position. The force in the X-direction is denoted FX in the figures, in the Y-direction FY and in the Z-direction FZ. The moment around the X-axis is denoted MX in the figures, around the Y-axis, MY, and around the Z-axis, MZ.

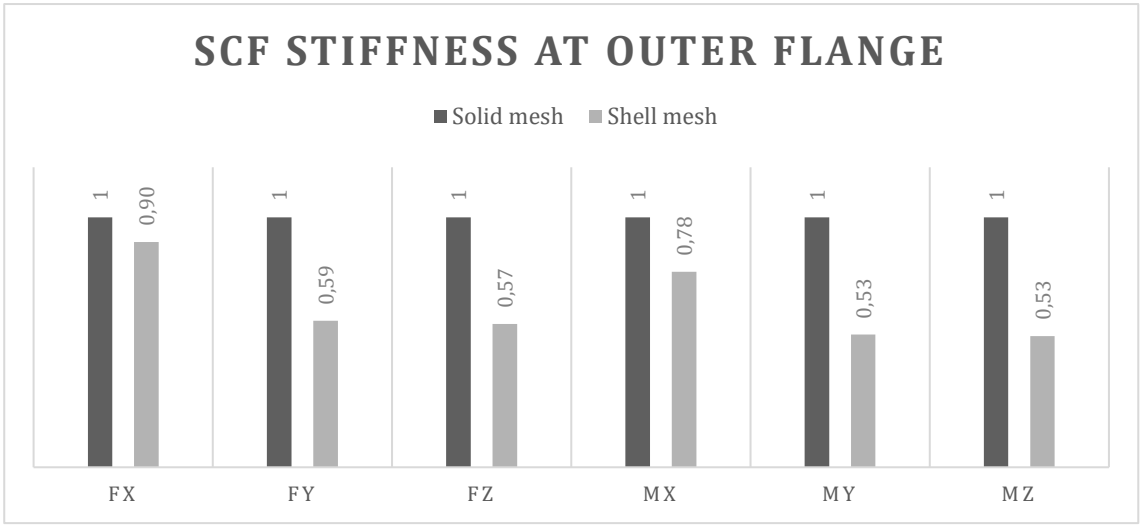

Figure 24: Stiffness comparison at the outer flange of the SCF, when keeping the front flange fixed. Stiffnesses are normalized with the respective stiffness of the solid model.

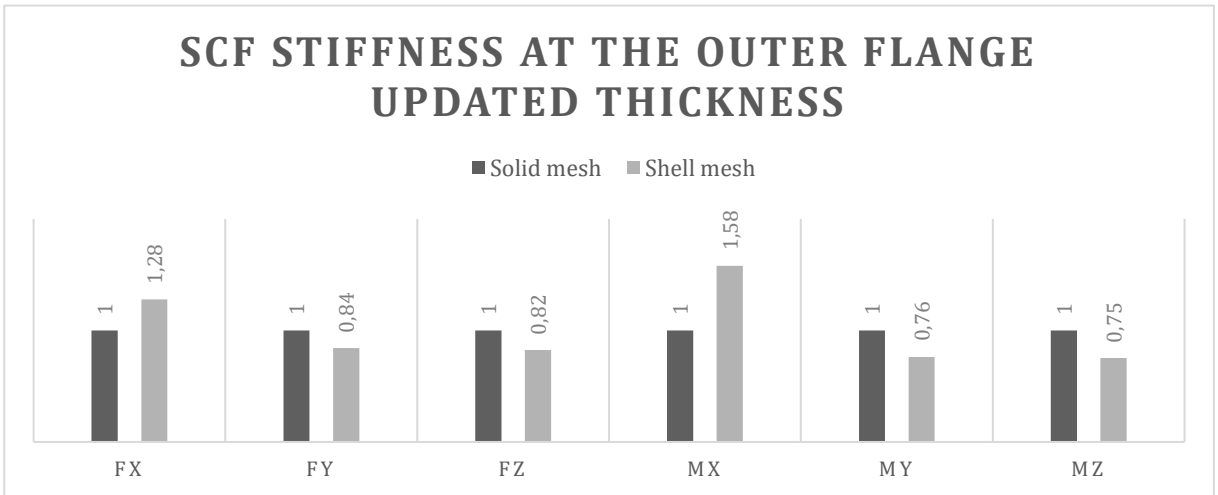

Figure 25: Stiffness comparison at the outer flange of the SCF, when keeping the front flange fixed, after a 40% thickness increment. Stiffness are normalized with the stiffness of the solid model.

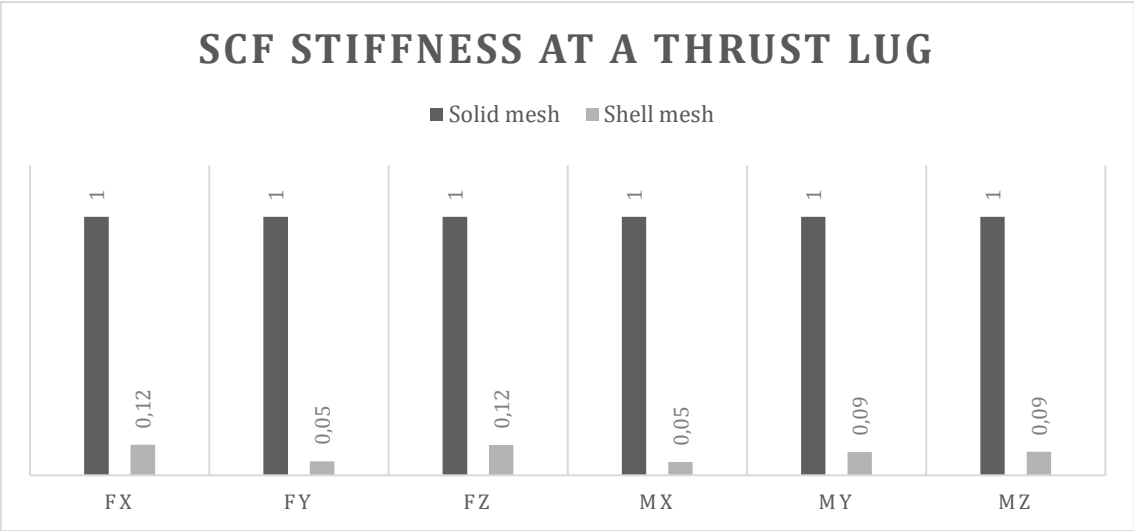

Figure 26: Stiffness comparison at a thrust lug of the SCF, when keeping the front flange fixed. Stiffnesses are normalized with the stiffness of the solid model.

7.2 Sanity Check of a Fan Blade

The shell meshed fan blade has a mass that is 86% of the mass of the solid meshed fan blade. The displacement field in the Z-direction, i.e. the radial direction, and the magnitude of the displacement over the shell-meshed blade for the case with a force applied at the tip of the fan blade can both be seen in Figure 27. The same plots, but for the centrifugal force, i.e. the force implemented with the RFORCE load card in OptiStruct, can be seen in Figure 28. The corresponding plots for the solid meshed blade can be seen in Figure 30 and Figure 29, respectively.

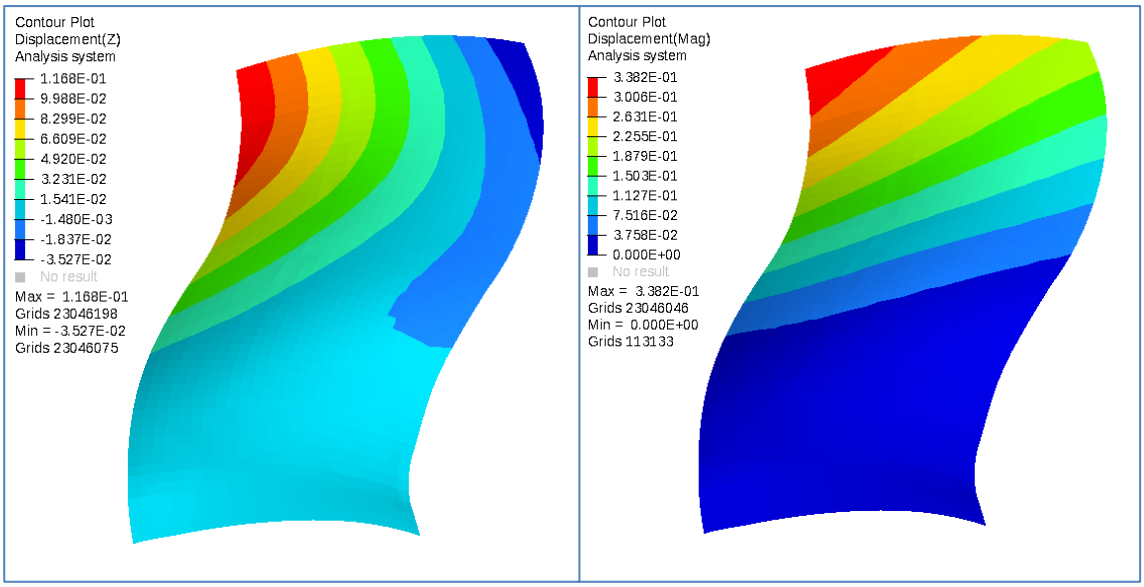

Figure 27: Displacement in the radial direction (left) and the magnitude of the displacement (right) from the force applied to the tip of the fan blade for the shell meshed fan blade with constant thickness.

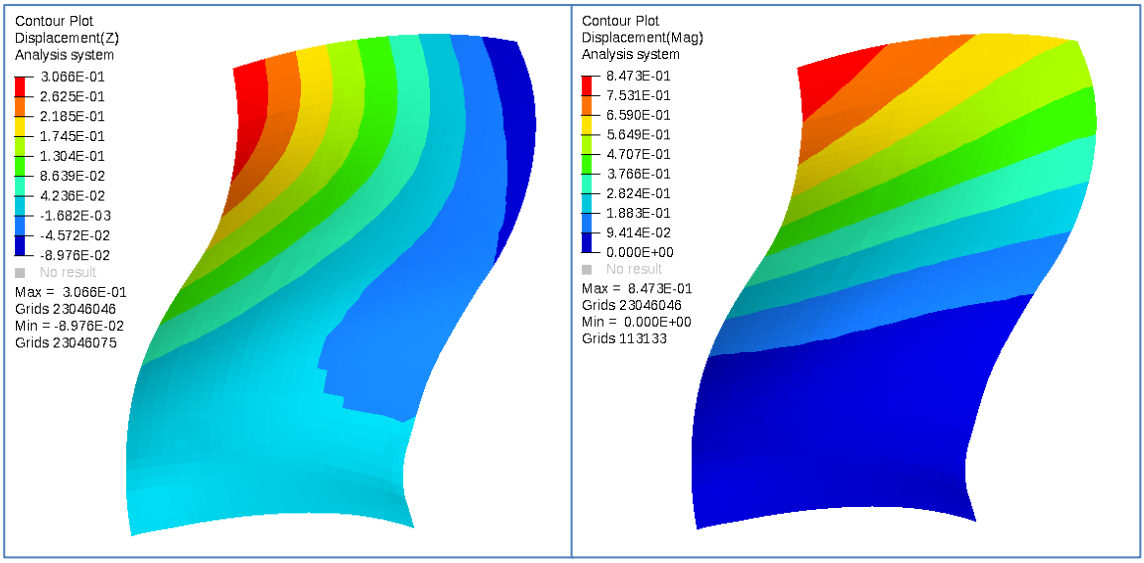

Figure 28: Displacement in the radial direction (left) and the magnitude of the displacement (right) from the centrifugal force for the shell meshed fan blade with constant thickness.

The maximum displacement in the radial direction for the shell meshed fan blade with constant element thickness is $117mm$ when the blade is subjected by the force applied at the tip of the fan blade and $307mm$ when directly subjected to the rotational acceleration field, resulting in a centrifugal force, which is 14% respectively 35% of the original fan blade length. The corresponding maximum displacement from the tip applied force is 338mm and 847mm for the centrifugal force.

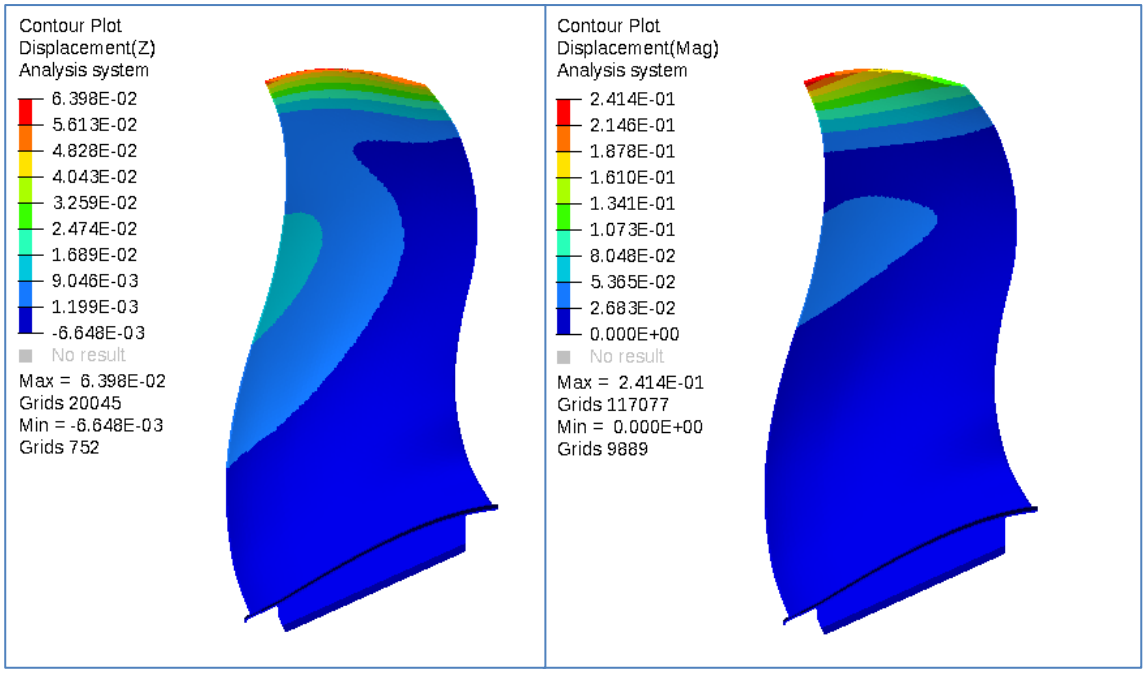

Figure 29: Displacement in the radial direction (left) and the magnitude of the displacement (right) from the force applied to the tip of the fan blade for the solid meshed fan blade.

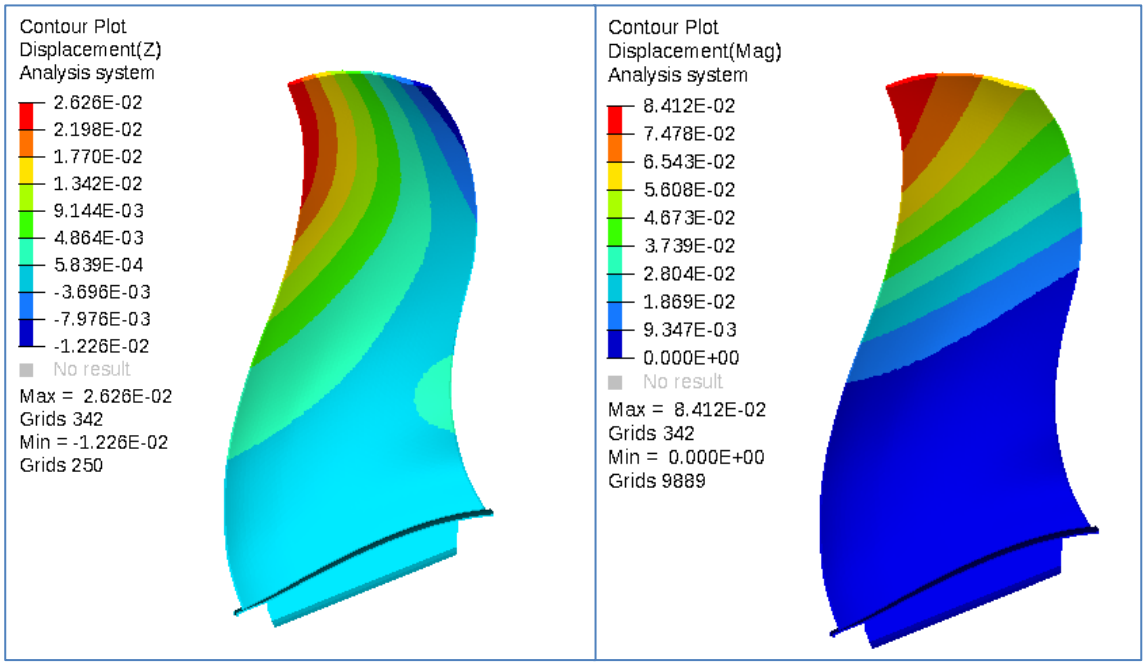

Figure 30: Displacement in the radial direction (left) and the magnitude of the displacement (right) from the centrifugal force for the solid meshed fan blade.

The maximum displacement in the radial direction for the solid meshed fan blade is $64mm$ when the blade is subjected to the force applied to the tip of the fan blade and $26mm$ when directly subjected to the rotational acceleration field, resulting in a centrifugal force, which is 3% respectively 8% of the original fan blade length. The corresponding maximum displacement magnitude from the tip applied force is 241mm and 84mm for the centrifugal force.

When the thickness of the shell meshed fan blade was updated to a tapered shape, the displacement distribution of the fan blade consequently changed compared to the

shell meshed fan blade with constant thickness. The displacement distribution can be seen in Figure 31 and Figure 32.

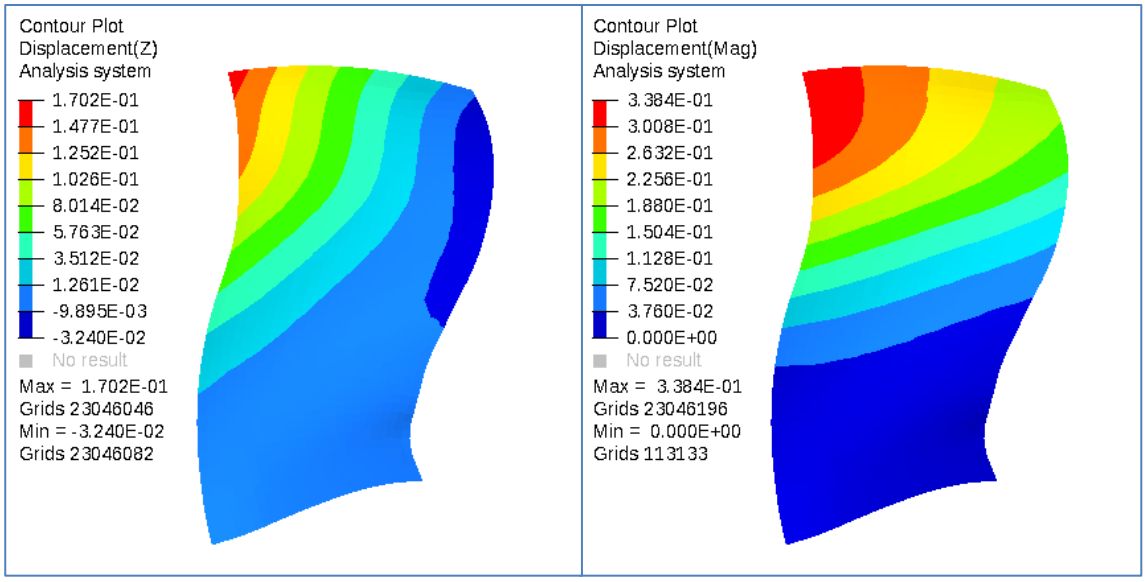

Figure 31: Displacement in the Z-direction (left) and magnitude of the displacement (right) due to the force applied to the tip of the fan blade for the shell meshed fan blade with tapered thickness distribution.

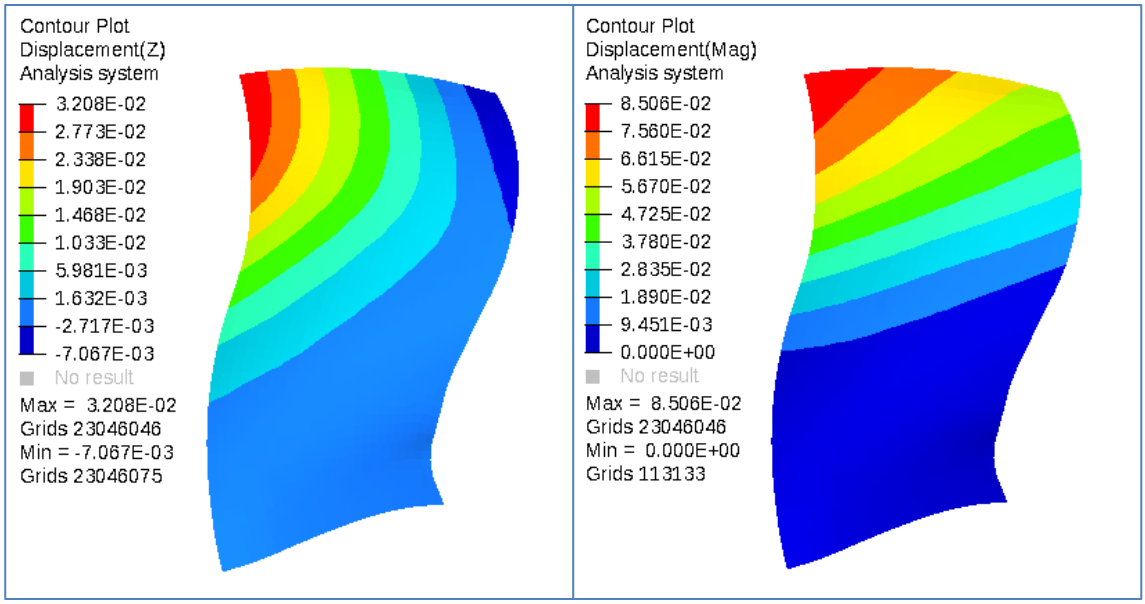

Figure 32: Displacement in the radial direction (left) and the magnitude of the displacement (right) due to the centrifugal force for the shell meshed fan blade with tapered thickness distribution.

The maximum displacement in the radial direction for the shell meshed fan blade with tapered thickness distribution is $170mm$ when the blade is subjected to the force applied at the tip of the fan blade and $32mm$ when directly subjected to the rotational acceleration field, resulting in a centrifugal force, which is 20% respectively 4% of the original fan blade length. The corresponding maximum displacement from the distributed force is $338mm$ and $85mm$ for the centrifugal force.

The simplified fan blade has a mass that is 69% of the mass of the shell meshed fan blade with constant thickness. The maximum displacement in the radial direction of

the simplified fan blade is $0.46mm$ for the force applied to the tip section and $0.29mm$ for the case with the force due to the rotation of the blade. The displacement field over the fan blade for both load cases can be seen in Figure 33.

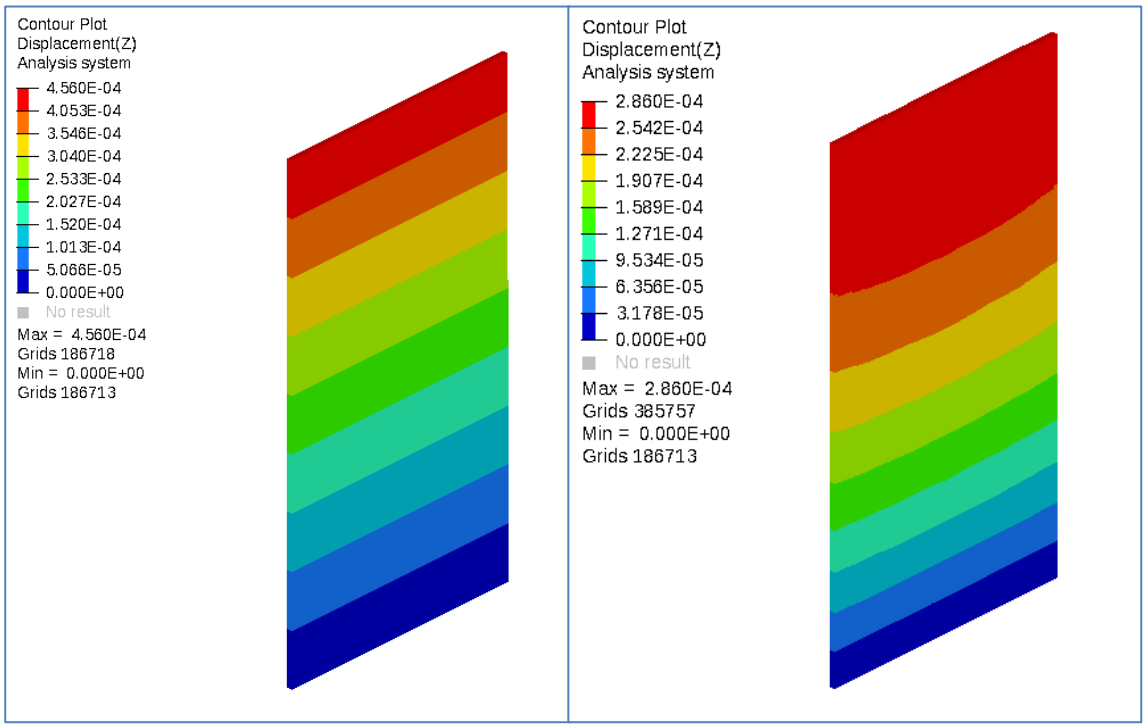

Figure 33: Displacement in the Z-direction of the simplified fan blade, due to the tip applied force (left) and due to the centrifugal force (right).

7.3 Design Load Cases

The displacement fields of the magnitude of the WEM are presented in this section. At first, the displacement fields of the WEM with original thickness are presented, i.e. the initial assumption of thicknesses. Thereafter, the displacement fields of the WEM with updated thicknesses are presented, i.e. when the thickness of all casings are increased with 40%. After the thickness increment, the density was altered so that the total weight of the model still matches the estimated weight of the Notional Engine.

7.3.1 "Original" Thickness

The maximum displacement magnitude for each load case for the WEM with original thicknesses can be seen in Table 3. The corresponding displacement fields can be seen in Figure 34 through Figure 44, where the graphical displacements have been magnified ten times. The unit for the displacement field in the figures is meters.

Table 3: Maximum displacement magnitude for each load case for the WEM with original thicknesses.

NUMBER	MAXIMUM DISPLACEMENT MAGNITUDE [MM]	REPRESENTS
1	113.60	Cruise thrust, no g-loads
2	111.10	-3g along vertical axis
3	90.59	1.5g along transverse axis
4	90.59	-1.5g along transverse axis
5	145.70	-3g along vertical axis + 1.5g along transverse axis
6	144.60	-3g along vertical axis - 1.5g along transverse axis
7	117.60	-3g along vertical axis + Cruise thrust
8	194.90	1.5g along transverse axis + Cruise thrust
9	75.18	-1.5g along transverse axis + Cruise thrust
10	197.50	-3g along vertical axis + 1.5g along transverse axis + Cruise thrust
11	80.85	-3g along vertical axis - 1.5g along transverse axis + Cruise thrust

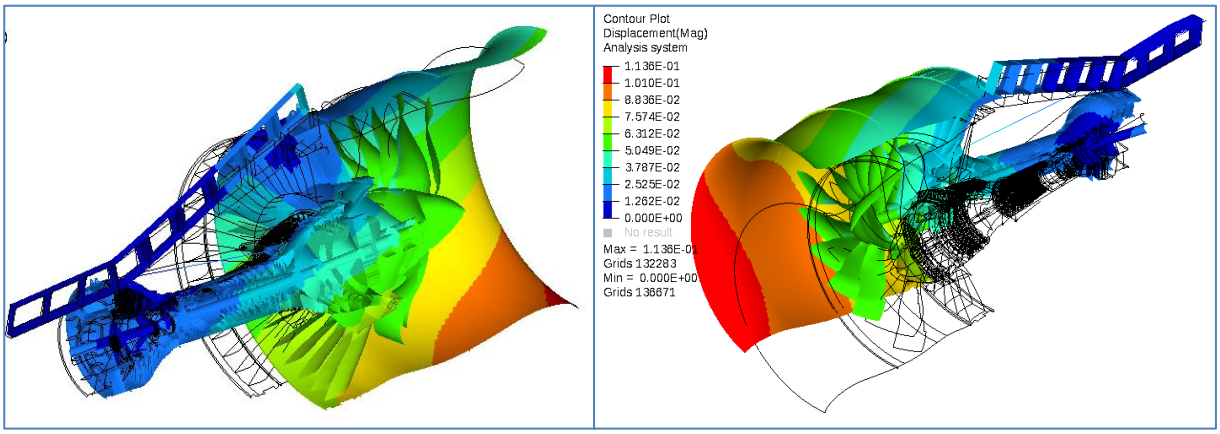

Figure 34: WEM displacement field for the original thickness distribution and load case 1: Cruise thrust, no g-loads.

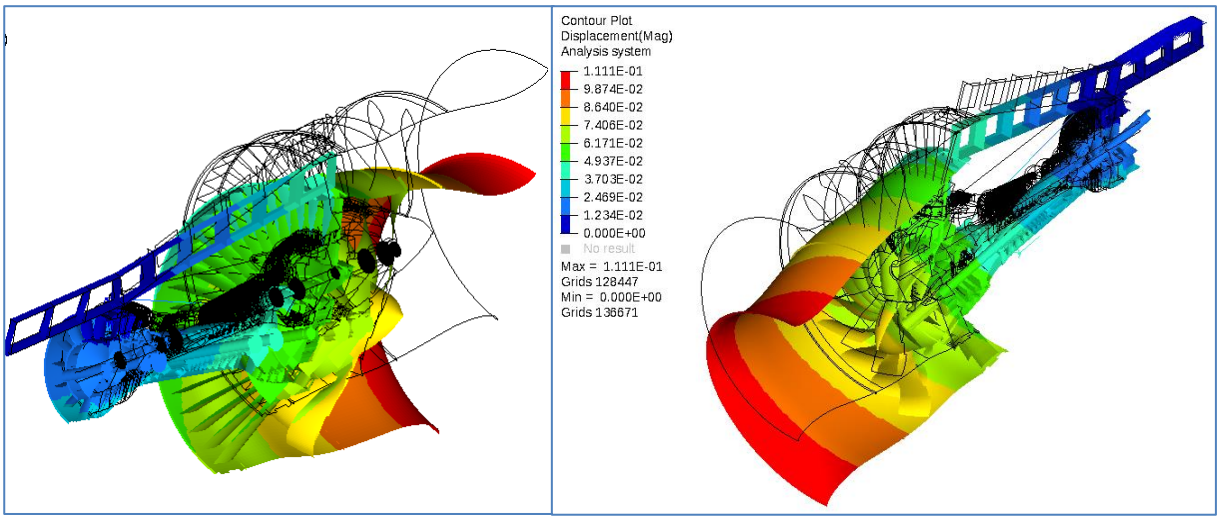

Figure 35: WEM displacement field for the original thickness distribution and load case 2: -3g along vertical axis.

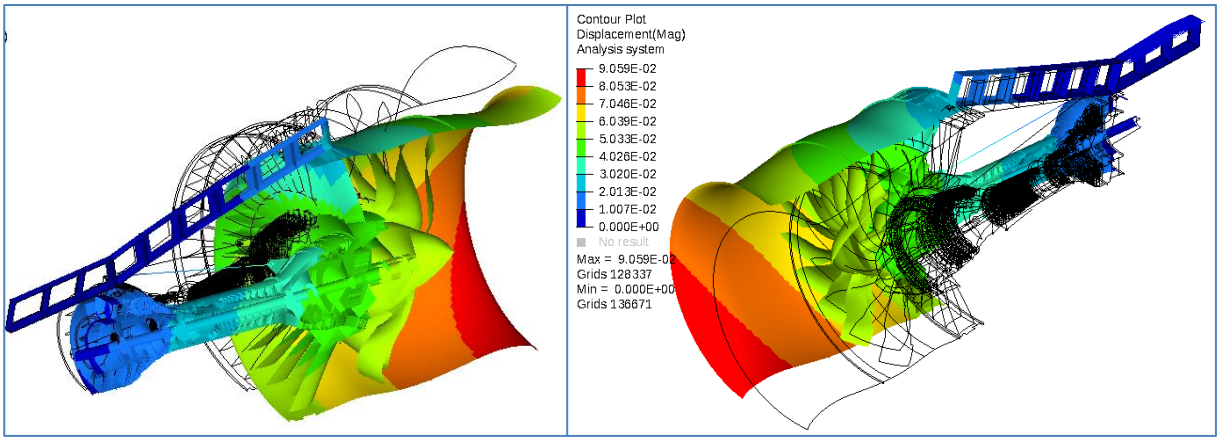

Figure 36: WEM displacement field for the original thickness distribution and load case 3: 1.5g along transverse axis.

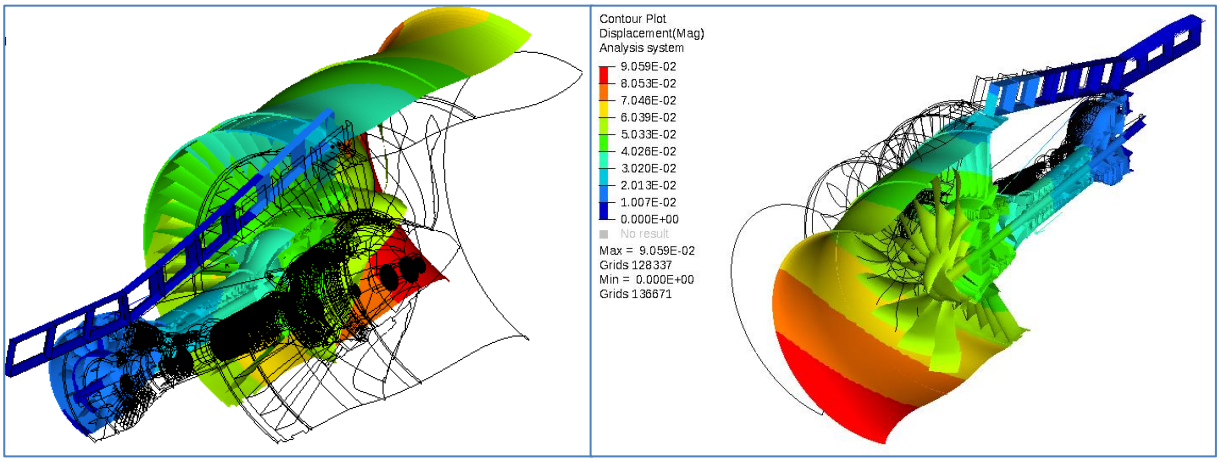

Figure 37: WEM displacement field for the original thickness distribution and load case 4: -1.5g along transverse axis.

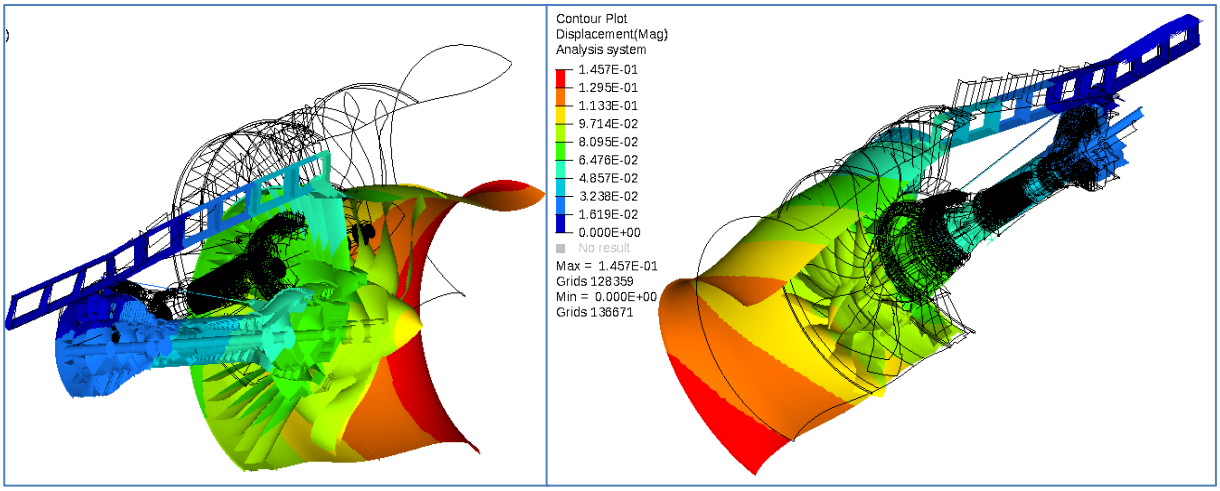

Figure 38: WEM displacement field for the original thickness distribution and load case 5: -3g along vertical axis + 1.5g along transverse axis.

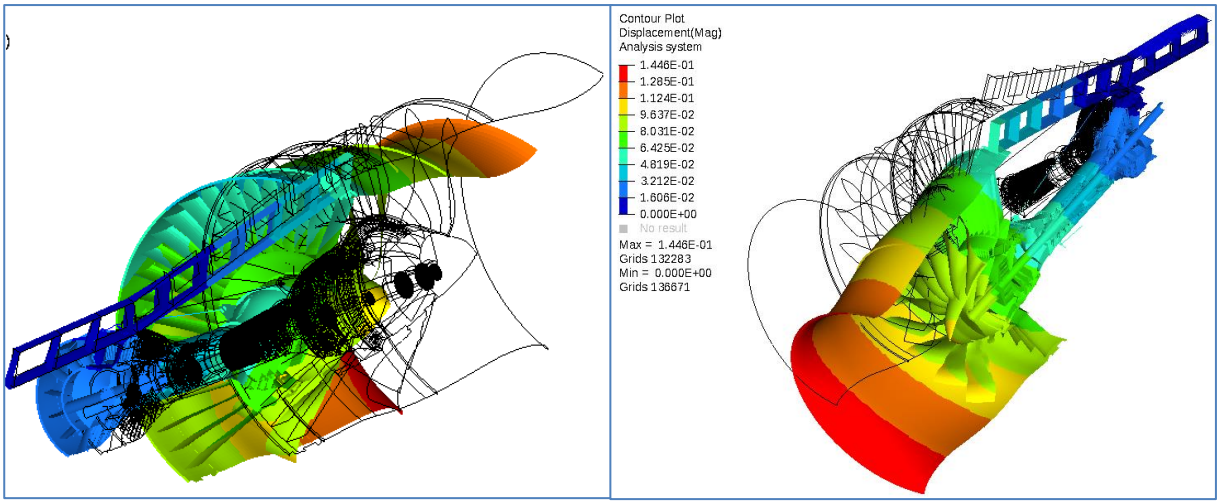

Figure 39: WEM displacement field for the original thickness distribution and load case 6: -3g along vertical axis - 1.5g along transverse axis.

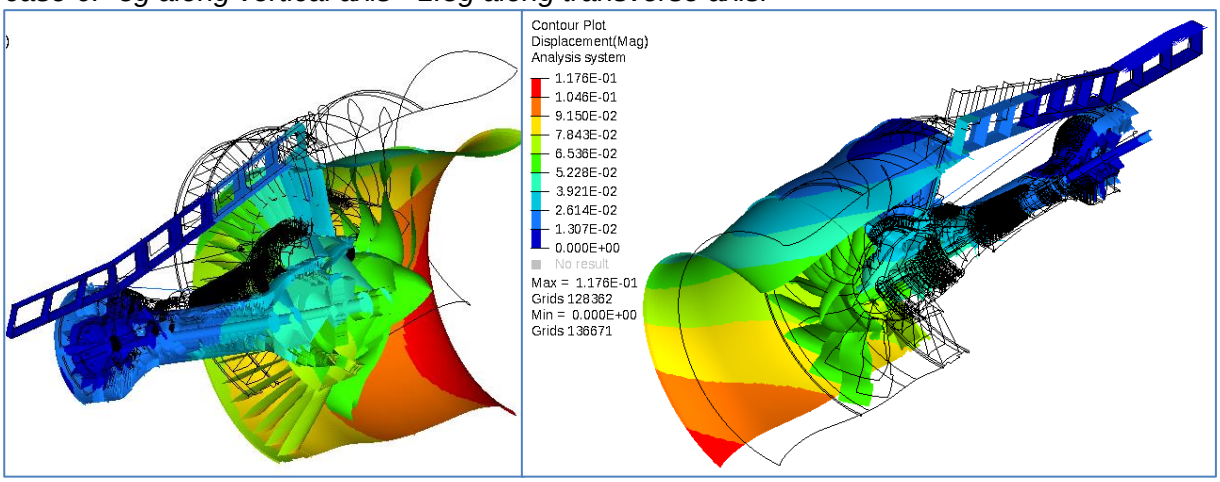

Figure 40: WEM displacement field for the original thickness distribution and load case 7: -3g along vertical axis + Cruise thrust.

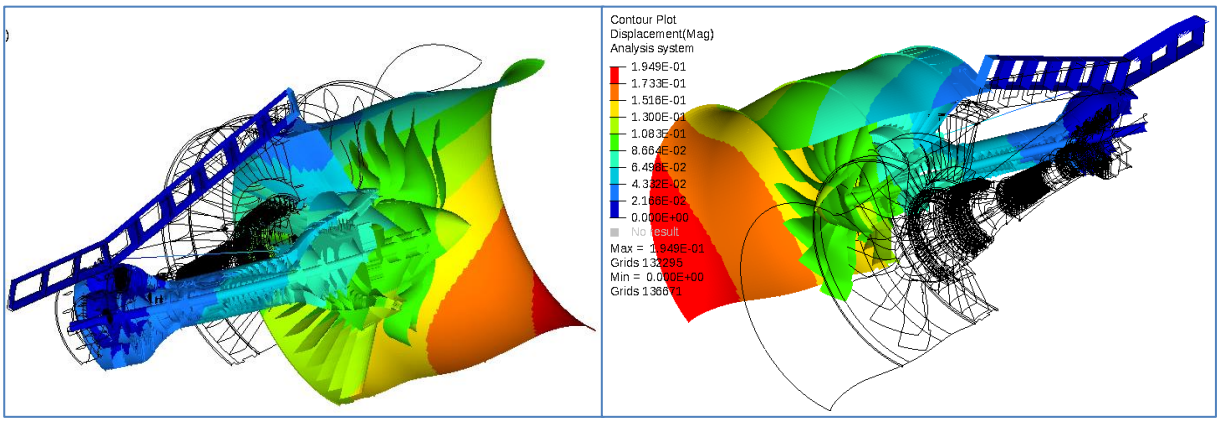

Figure 41: WEM displacement field for the original thickness distribution and load case 8: 1.5g along transverse axis + Cruise thrust.

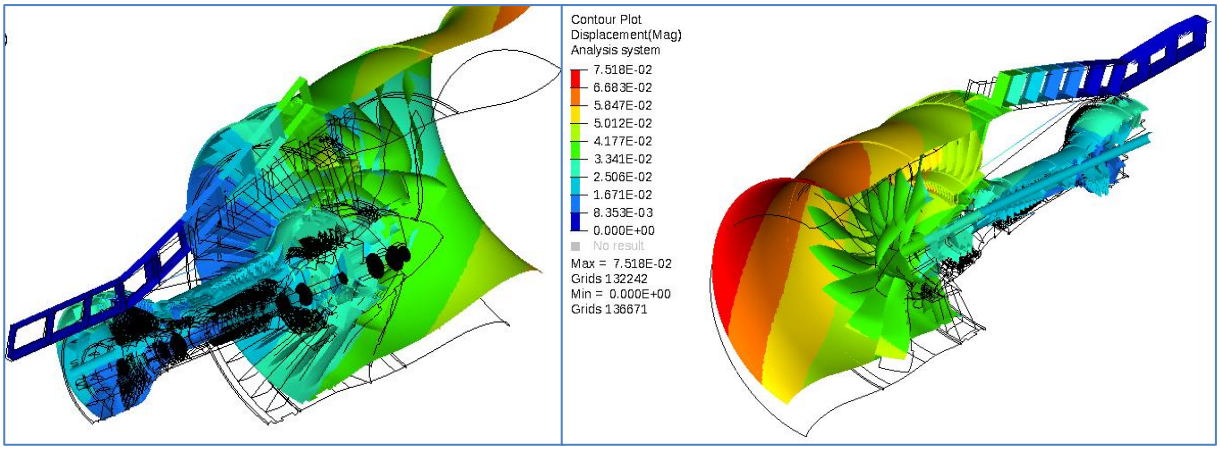

Figure 42: WEM displacement field for the original thickness distribution and load case 9: -1.5g along transverse axis + Cruise thrust.

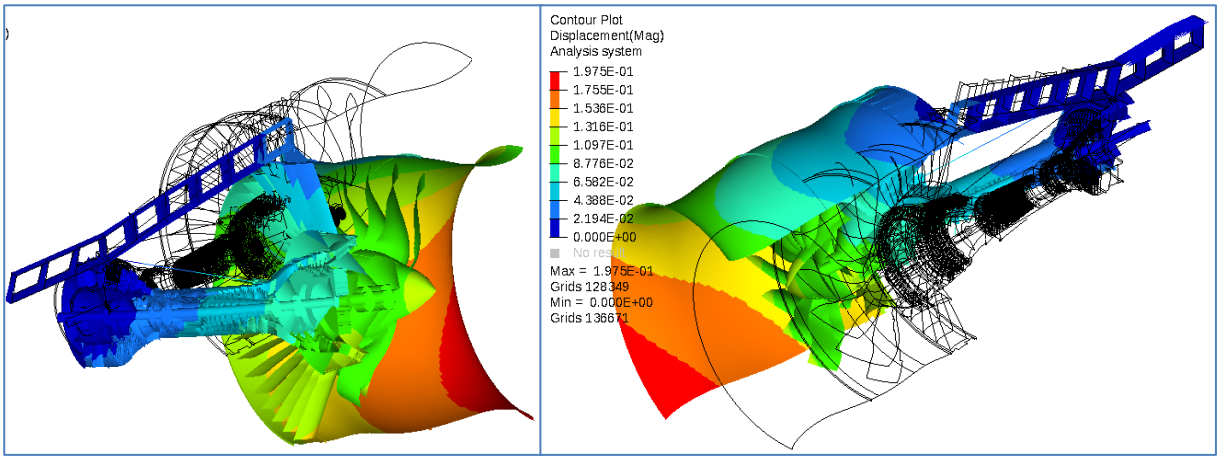

Figure 43: WEM displacement field for the original thickness distribution and load case 10: -3g along vertical axis + 1.5g along transverse axis + Cruise thrust.

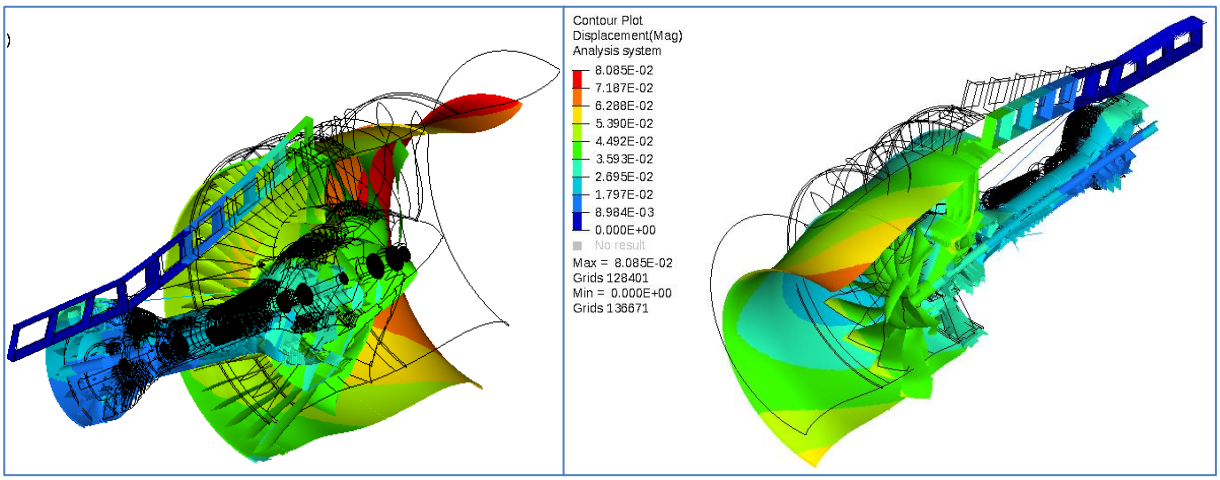

Figure 44: WEM displacement field for the original thickness distribution and load case 11: -3g along vertical axis - 1.5g along pitch axis + Cruise thrust.

7.3.2 New Thickness of Selected Components

The maximum displacement magnitude for each load case for the WEM with updated thicknesses can be seen in Table 4. The displacement field these load cases can be

seen in Figure 45 through Figure 55, where the graphical displacements have been magnified ten times. The unit for the displacement field in the figures is meters.

Table 4: Maximum displacement magnitude for each load case for the WEM with original thicknesses.

NUMBER	MAXIMUM DISPLACEMENT MAGNITUDE [MM]	REPRESENTS
1	117,40	Cruise thrust, no g-loads
2	107,10	-3g along vertical axis
3	78,83	1.5g along transverse axis
4	78,83	-1.5g along pitch axis
5	134,50	-3g along vertical axis + 1.5g along transverse axis
6	133,70	-3g along vertical axis - 1.5g along transverse axis
7	119,60	-3g along vertical axis + Cruise thrust
8	187,60	1.5g along transverse axis + Cruise thrust
9	77,00	-1.5g along transverse axis + Cruise thrust
10	189,10	-3g along vertical axis + 1.5g along transverse axis + Cruise thrust
11	80,58	-3g along vertical axis - 1.5g along transverse axis + Cruise thrust

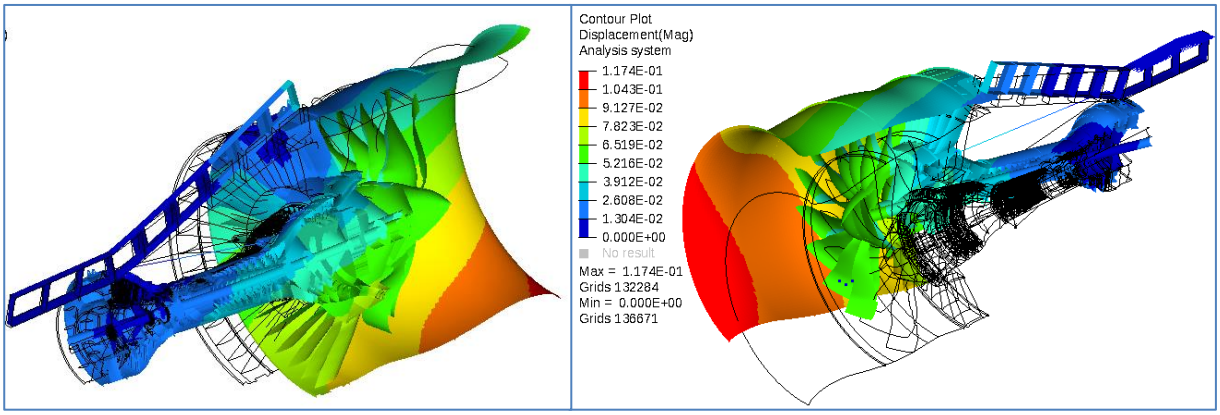

Figure 45: WEM displacement field for the updated thickness distribution and load case 1: Cruise thrust, no g-loads.

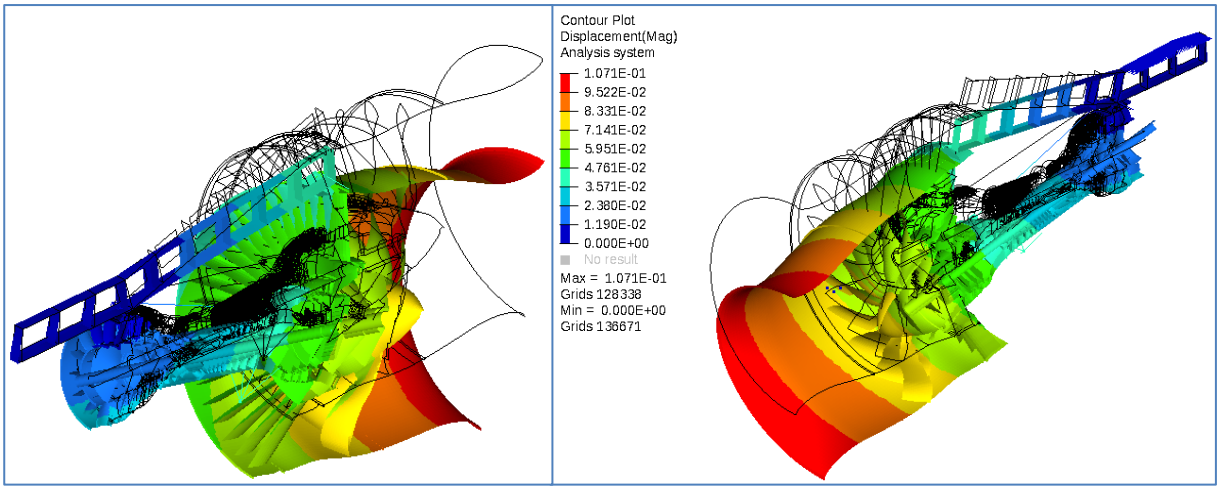

Figure 46: WEM displacement field for the updated thickness distribution and load case 2: -3g along vertical axis.

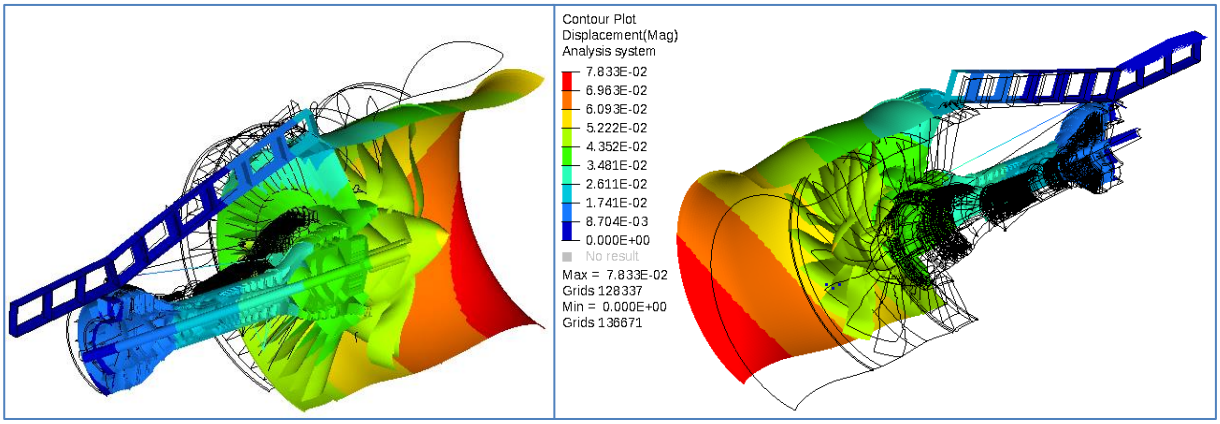

Figure 47: WEM displacement field for the updated thickness distribution and load case 3: 1.5g along transverse axis.

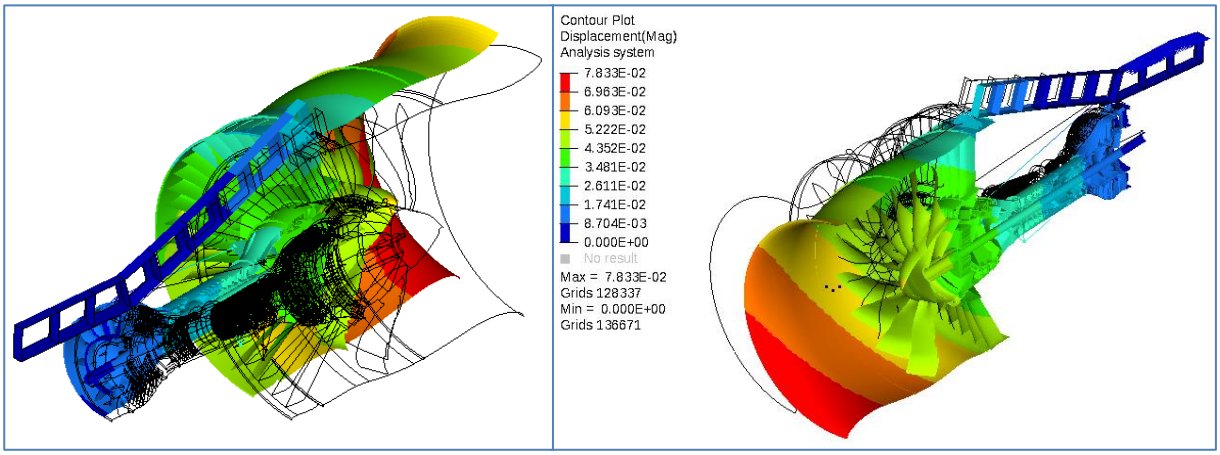

Figure 48: WEM displacement field for the updated thickness distribution and load case 4: -1.5g along pitch axis.

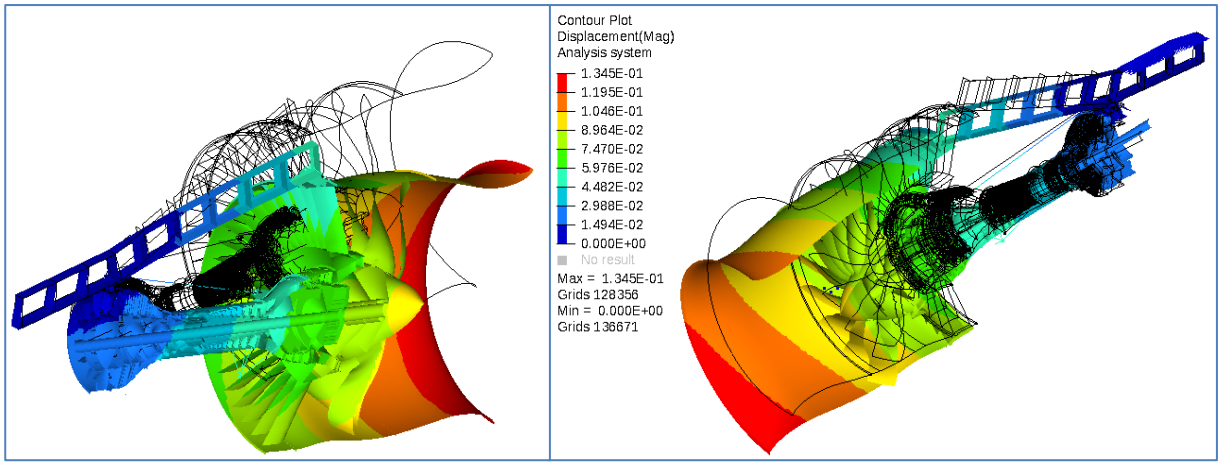

Figure 49: WEM displacement field for the updated thickness distribution and load case 5: -3g along vertical axis + 1.5g along transverse axis.

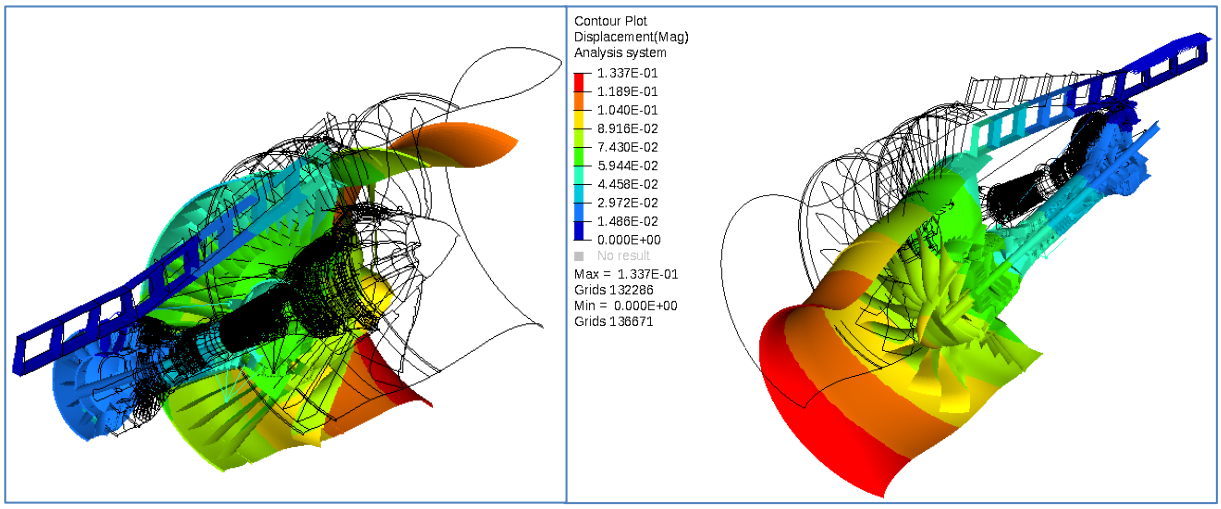

Figure 50: WEM displacement field for the updated thickness distribution and load case 6: -3g along vertical axis - 1.5g along transverse axis.

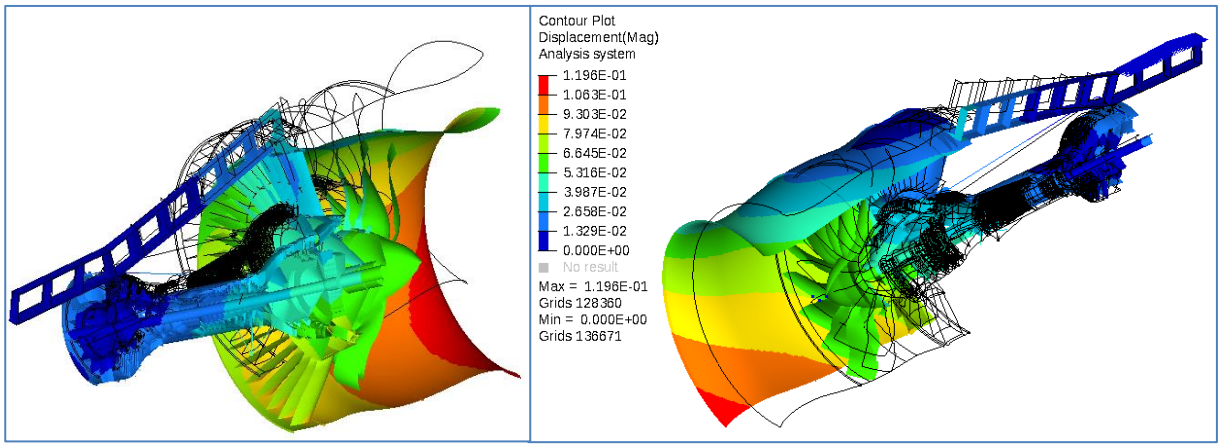

Figure 51: WEM displacement field for the updated thickness distribution and load case 7: -3g along vertical axis + Cruise thrust.

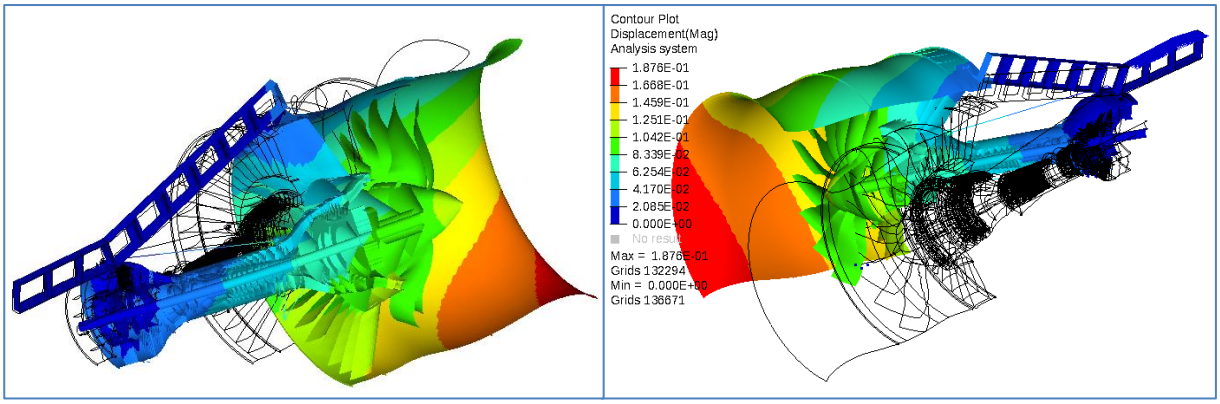

Figure 52: WEM displacement field for the updated thickness distribution and load case 8: 1.5g along transverse axis + Cruise thrust.

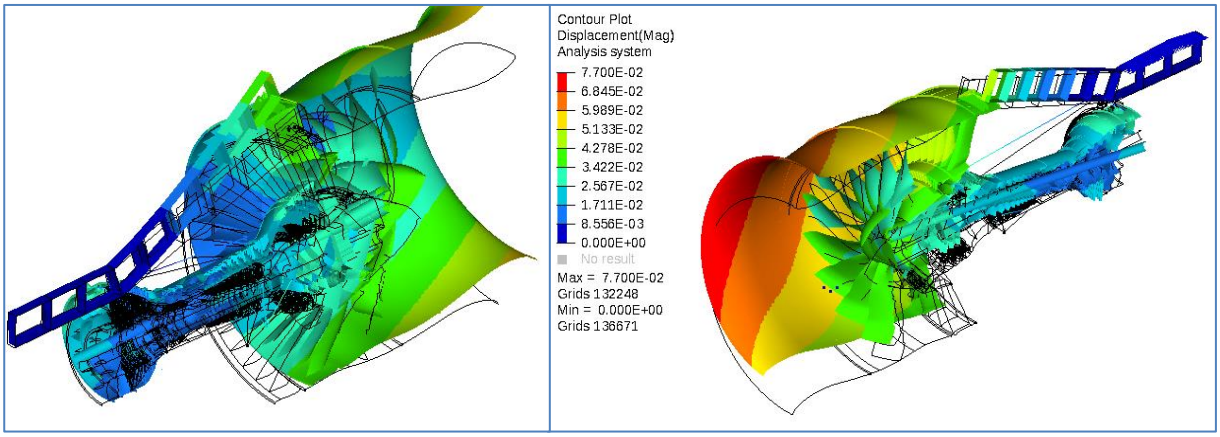

Figure 53: WEM displacement field for the updated thickness distribution and load case 9: -1.5g along transverse axis + Cruise thrust.

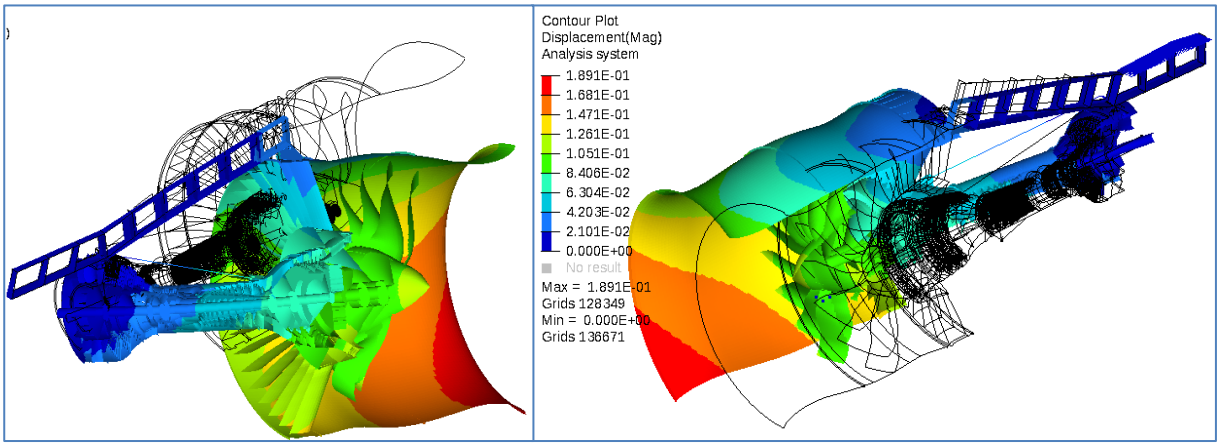

Figure 54: WEM displacement field for the updated thickness distribution and load case 10: -3g along vertical axis + 1.5g along transverse axis + Cruise thrust.

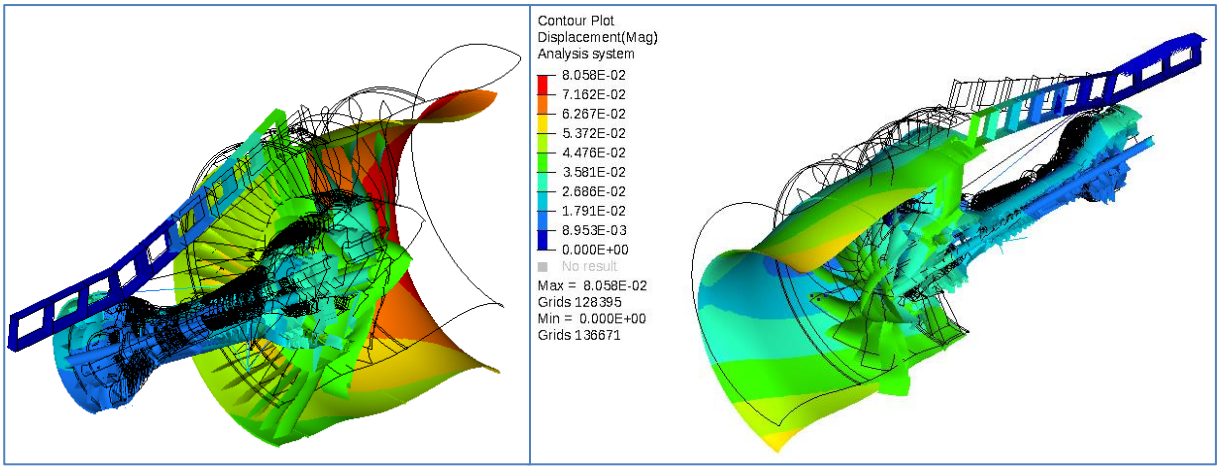

Figure 55: WEM displacement field for the updated thickness distribution and load case 11: -3g along vertical axis - 1.5g along transverse axis + Cruise thrust.

8 Discussion

The results from the sanity check and the results from the different load cases are analyzed in this section.

8.1 Sanity Check Structural Compressor Frame

It can be seen that the shell model of the SCF has a much lower mass than the solid model of the same geometry. The shell model is still 12% lighter than the solid model after increasing the density by 40%. The loss of mass is assumed to occur due to geometrical simplifications and the fact that the shell model is smaller than the solid model. Why the shell model is smaller is hard to tell, but a plausible assumption for a part of the shrinkage is that it is occurring during the transformation from the solid model to the mid-surface model used for the shell mesh. However, this cannot explain the so large loss of mass. It is also likely that the geometrical representation of the element thickness used in the shell model needs to be altered and modelled with higher fidelity to better represent the solid model.

From Figure 24 it can be seen that the shell model has a lower stiffness than the solid model at the outer flange connecting the SCF to the LPC. Best stiffness correlation occurs for the force in X-direction and the moment around the X-axis.

From Figure 25 it can be seen that the stiffness is better correlated after a thickness increment of the inner and outer casings of the SCF. All measured stiffnesses, except for the moment around the X-axis is within 30 percentage. This stiffness correlation may be a good enough correlation between the shell and solid model for early stage engine development. A better stiffness correlation can most definitely be obtained by optimization of different parameters, such as Young's modulus, density, thicknesses of element, et cetera, as Raja [2] especially focused in a previous thesis project at GKN. This will result in a more accurate WEM and enable more accurate BCs for sub-component analysis, and thus, give better opportunities for an improved engine design and is strongly recommended for later stages of engine development.

From Figure 26 it can be seen that shell model has significantly lower stiffness than solid model at the thrust lugs. The poorest match for stiffness response is obtained for the force in Y-direction and the moment around the X-axis. The same improvements with increased thicknesses were not observed for the thrust lugs, as for the outer flange. Optimization of different material parameters may, most likely, not cause good enough results either.

By taking a closer look at the thrust lugs of the solid meshed SCF in Figure 16 and the thrust lugs of the shell meshed SCF in Figure 17, some differences may be observed. The thrust lugs in the solid model have stiffeners between them and the SCF casing, and the geometry indicates a significantly more robust structure near the SCF outer case. The lugs on the shell model are modeled as two sheets without any stiffener between them and lack the robustness close to the SCF outer case. The lugs at the solid model also have a different shape and appear to have a larger contact area to the SCF outer case, compared with the lugs at the shell model. In conclusion, the lugs at the shell model appear not to represent the lugs of the solid model and are most likely too simplified. This is likely the causing of the poor stiffness correlation between the lugs of the shell and solid model.

8.2 Sanity Check Fan Blade

From Figure 27 and Figure 28 it can be seen that both the tip applied force and the centrifugal force give very large displacements for the shell meshed fan blade with constant thickness distribution . By studying the displacements in radial direction, it can be observed that the maximum displacement for the tip applied force corresponds to 14% of the original fan blade, whereas for the centrifugal force implemented with the RFORCE load card results in 35%. Both these displacements appear to be too large and non-physical for a true engine behavior, which is confirmed by experienced engineers at GKN.

From Figure 30 and Figure 29 it can be seen that the magnitude of the displacement of the solid meshed fan blade is within range of what is more plausible compared to the shell meshed fan blade with constant thickness. Applying the normal force present at the hub section due to the rotation of an object at the tip of the fan blade should give an overestimation of the displacement. However, this is not the case for the studied blade and the tip applied force gives smaller displacement. This may be due to the curved blade. It appears that the curved blade wants to straighten when subjected to the centrifugal force, and thus, gets a larger radial displacement.

By comparing the results from the shell meshed fan blade with constant thickness and the results from the solid meshed fan blade, it can be observed that the shell model with constant thickness do not represent the mechanical behavior of the solid meshed model. It can also be observed that the mass of the shell model with constant thickness is lower than the solid model. A lower mass gives a lower rotational force, which should result in a lower displacement of the shell meshed fan blade with constant thickness. However, a larger thickness at the bottom of the fan blade gives more stiffness to the blade than it increases the rotational force, which may explain the closer to expected behavior of the solid meshed fan blade.

By studying Figure 31 and Figure 32, it can be observed that the shell meshed fan blade with tapered thickness gives displacements that are quite similar to the solid meshed fan blade for the centrifugal load. While the distributed force at the tip of the fan blade gives distinguishable larger deformations. The maximum normal force at the shell meshed fan blade with varying thickness is heavier than the shell meshed fan blade with constant thickness, which means that the normal force is larger, and thus, the tip applied force. The tip applied force is an overestimated force and since the tapered fan blade is weaker further to the tip, the displacement becomes rather large. Therefore, it can be concluded that the current estimation of the centrifugal force was not accurate.

By comparing the displacement fields that occurs due to the centrifugal force for the solid meshed fan blade and the shell meshed fan blade with tapered thickness, it can be observed that the displacement fields have a similar appearance. Since it captures both the displacement field and the magnitude of the displacement of the centrifugal force, it is fair to say that the updated shell meshed fan blade with tapered thickness captures the behavior of the solid meshed fan blade. Needless to say, simplifying rotating blades with large tapering and low hub-to-shroud diameter ratio such as fan blades to a constant thickness is a much too crude simplification. These gyroscopic loads from turning would be affected from such a too crude simplification. Furthermore, to accurately simulate run-down unbalance and windmilling after a blade-off event it would be important to get the mass distribution representative to

obtain representative unbalance loads. For blades with less tapering and higher hub-to-shroud diameter ratios, a constant thickness simplification is likely not as bad of an assumption.

From Figure 33 it can be seen that the displacement of the simplified fan blade due to the tip applied force is larger for the FEM solution than the simplified hand calculations. This is expected since the maximum normal force in the blade, i.e. from the hub, is applied to the tip, and thus, lead to a uniform stress profile along the blade at the true max stress level, whereas the true case from the centrifugal force has this maximum stress in the hub and none at the tip. It can also be observed that the centrifugal force gives a smaller displacement than the tip applied force, but a larger displacement than for the hand calculations in Appendix iii. The displacement in the hand calculations is a purely 1D problem where the area of the blade is assumed to remain constant. While the FEM calculations is a 3D problem where the area of the blade can shrink. Since the area shrinks in the FEM problem, the normal forces in the blade increases, and thus, the displacement of the blade increases. When the simplified blade is exposed to rotational forces, it should stretch in the radial direction and its cross-sectional area should shrink. Therefore, we can conclude that the hand calculations overestimate the stiffness of the blade, and thus, underestimate the displacement of the blade. It can therefore be concluded that the RFORCE load card in OptiStruct, if implemented correctly, seems to produce trustworthy results for for solid elements.

By comparing the results from the centrifugal force at the solid meshed fan blade with the simplified fan blade, it can be observed that solid meshed fan blade gets a much larger deformation. This larger deformation is assumed to occur due to the geometry of the fan blade. The fan blade untwists, which moves surface of the fan blade away from its centre of gravity and additionally, the fan blade have different product of inertia. This may cause another load distribution over the fan blade that gives larger deformations. The solid meshed fan blade is curved, and thus, wants to straighten, which means that the displacement in the radial direction may grow. The simplified fan blade has its centre of gravity in its geometrical centre and such effect may therefore not appear on the simplified blade. The simplified blade is also already straightened. In conclusion, it can be confirmed that the RFORCE card is functional for the solid mesh of the fan blade, and therefore, functional for the shell mesh of the fan blade with varying thicknesses. However, so large displacement for the true fan blade is something that should be further investigated.

In brief, the questionable results from the preliminary assessment of forces due to rotating parts at the WEM were indeed inaccurate when a constant thickness was used at the blades. A more accurate displacement field of the fan blade was obtained when a varying thickness was used for the fan blade. Therefore, it is recommended to have varying thickness over the blades, as in the solid model of the fan blade, to obtain more accurate results of the displacements due to rotation.

8.3 Whole Engine Model Design Load Cases

Worth to have in mind before analyzing the loads on the WEM is that the stiffness of the shell-meshed components may not be optimal compared to if they would have been meshed with solid elements, as discussed in Section 8.1. The stiffness may most likely be too low, which was the case for the shell meshed SCF.

In addition, it is also worth to have in mind that all blades (fan, compressor and turbine blades) are modeled with a constant thickness, since assumption for constant thickness distribution along the blade showed to be inadequate during a later stage of the project. However, as no rotational loads were included among the load cases the impact on the results presented below should be limited.

8.3.1 "Original" Thickness

From Table 3 it can be seen that load case 3 and 4 give the same displacement magnitude, which is quite predictable since the engine is almost symmetrical along the vertical axis and that the gravitational loads have the same magnitude, but acts in opposite directions. The same behavior can be seen for load case 5 and 6. Still, a small difference can be seen between the magnitudes. The non-symmetrically placed AGB may be the cause of the difference. Moreover, if the engine is exposed to purely gravitational load along the transverse axis, it makes no difference whether the gravitational load acts in the negative or positive direction. Only a small difference is obtained when a gravitation load along the vertical axis is added to the aforementioned load.

From Table 3 it can be seen that the largest displacement is obtained from load case 10, followed by load case 8. The load cases with smallest displacements are load case number 9, followed by load case number 11. It is quite interesting to see that both the largest and the smallest displacements occur when the thrust force is combined with gravitational loads. It can seem expected that the maximum displacement occurs for either load case 10, or 11, since the engine is subjected to the most different kinds of loads during these load cases. However, that load case 11 gives the second smallest displacement is far from expected. It appears that the different load contributions counteract each other.

By studying Figure 34 it can be seen that thrust force increases the displacement in the negative longitudinal direction, due to the acting thrust force, and in the positive transverse and vertical direction of the engine, due to the moment applied at the fan gearbox. From Figure 35 it can be seen that the negative gravitational load along the vertical axis increases the displacement in the negative vertical direction and the negative roll direction. That this load does not displace the engine purely along the vertical axis is presumably due to the non-symmetrically placed AGB. By comparing Figure 34 with Figure 35 and studying the displacement field of load case 7 in Figure 39, it can be seen that the cruise thrust gives more displacement than along the transverse axis than 3g in the negative vertical direction.

When a gravitational load acting along the transverse axis is added to the cruise thrust, as in load case 8 and 9, or to the cruise thrust and the gravitational load along the vertical axis, as in load case 10 and 11, it either contributes or counteracts the displacement. In load case 8 and 10, the gravitational load along the transvers axis contributes to an increased displacement and in load case 9 and 11, it counteracts to the displacement.

By studying Figure 34 through Figure 44 it can be seen that the largest displacement occurs at the inlet for each load case. The inlet appears to curve more the further away from it goes the pylon, which is reasonable with the BC and model assumptions made for the WEM with the fixed latter part at the upper face of the pylon. However, the magnitude of the displacements appears to be rather large. Perhaps, stiffer components with inclusion of stiffening features that possibly better represent the real

Notional Engine, which showed to be the case for the investigated SCF component, could have stiffened up the engine as a whole, and therefore, reduced the displacement at the fan casing. Furthermore, it should also be noted that the pylon stiffness also could have a large effect on the displacements of the front of the engine. The design of the pylon can likely be optimized to minimize both displacements and reaction forces.

From Section 8.1, it is evident that the thrust lugs in the shell model are much weaker than the thrust lugs in the solid model. The thrust lugs are considered as quite stiff components in the real engine, which is not the case in the WEM. The thrust lugs and the thrust links are designed to carry the major part of the generated thrust force. However, the weak thrust lugs may struggle to carry the thrust force in the WEM, which may have a big impact on the stiffness and the load path through the engine. In other words, other components may have to carry the thrust force and the displacement field may not represent the displacement field for the set of designed components that the engine builds upon.

8.3.2 New Thickness of Selected Components

From Table 4 it can be seen that load case 3 and 4 gives the same displacement magnitude and that load case 5 and 6 have almost the same displacement magnitude, just as for the WEM with the original thicknesses. From the same table, it can be seen that the largest displacement is obtained from load case 10, followed by load case 8. The load cases with least displacements is load case number 9, followed by load case number 11. This is also in line with the WEM with the original thicknesses.

Small differences between the displacement magnitude of the WEM with constant thicknesses in Table 3 and the WEM with updated thicknesses in Table 4 were observed. The largest difference is obtained at load case 3 and 4, where the difference in magnitude is 15%. By comparing the displacement fields of the original and updated WEM, in Figure 34 through Figure 44 and Figure 45 through Figure 55 respectively, no obvious differences can be observed. Consequently, the increased stiffness of the inner and outer casings seems to do little to decrease and change the displacement field of the WEM.

From Section 8.1, it can be seen that the thrust lugs are much weaker in the shell model compared to the solid model. If the thrust lugs would have been updated to be stiffer as for the real geometry, instead of the inner and outer casings, then the displacement field might change. The same argument goes for other stiffeners that might have been excluded as discussed in Section 8.3.1.

9 Summary

- A general overview of the loads on an aero engine has been presented.
- A finite element model of the Notional Engine has been developed where all components have been individually meshed and assembled to a mechanical whole engine model.
- The whole engine model is prepared for extracting interfacial loads at the structural compressor frame.
- The sanity of the whole engine model has been investigated.
- A set of maneuver load cases has been implemented and analyzed at the whole engine model.
- The current WEM can be used as a building block towards achieving an accurate whole engine model, however, more work is needed to get an adequate WEM, and thus, get reliable load levels and displacements between the components.

10 Future Work

To capture an accurate structural behavior of the engine it would be key to study more components, as done for the SCF and the fan blade within this master's thesis, to assure that the shell models are representative of the underlying engine.

The thrust lugs in the WEM are not representative of the true thrust lugs. A first suggestion would be to investigate how to model the geometry of the thrust lugs in the shell model to be representative of the lugs in the solid model. A second suggestion would be to model the thrust lugs with solid elements, instead of using shell elements, to make sure that the thrust lugs in the WEM represent the lugs in the sub-component analysis of the SCF. On the other hand, this brings other difficulties that need to be considered, e.g. how to connect the solid meshed thrust lugs with the shell meshed casing.

Since the thrust lugs in the shell model were not representative, it is suggested to also investigate the lugs at the FCMR and the TRS.

The thicknesses of the blades in the WEM should be updated so that they represent the actual blades more correctly. Right now, the blades in the WEM have a constant thickness, which was found to be a much too crude simplification in Section 8.2.

The large displacement of the fan blades should be further investigated.

Updating the thicknesses of the blades in the WEM enables for more trustworthy displacement caused by the centrifugal forces, implemented with the RFORCE load card in OptiStruct. Introducing rotating parts in the engine enables for analysis of gyroscopic effects on the engine.

Finally, when an adequate WEM is obtained, more load cases should be implemented and analyzed. For each implemented load case, BCs should be obtained at each interface of selected components. The BCs could be obtained by centre line load transferring of loads at interfaces, e.g. obtained by the implemented CBUSH elements.

11 Things to Have in Mind for the Next Whole Engine Model

The current (June 2019) meshed WEM of the Notional Engine was created to ensure that the mesh quality was of adequate quality. To have the same number of elements at the interfaces between the components was somewhat not considered. On the other hand, to make the elements between the components to match is something that I would highly recommend for the next WEM. To have corresponding elements between the components was found to simplify the process of obtaining the interfacial loads, and thus, making it easier to obtain the BCs for sub-component analysis.

It is also recommended to carefully evaluate how to best represent each part of each component for the shell model, which was done for the current WEM. However, the goal with the simplifications was to capture the weight of the engine, not to capture the mechanical behavior of it. The mechanical behavior is something that I would strongly recommend to have in mind in the process of simplifying the solid model to a shell model, otherwise, the displacement field and the BCs would most likely be inaccurate, which might be the case of the current WEM.

A different approach when performing WEM analysis is to model the entire engine with solid elements. If doing so, some of the other necessary simplifications will not be needed and the room for error and need for assumptions in the simplification process is reduced. The reason behind using shell elements was to mimic the OEMs way of performing WEM analysis and to save computational time. However, the OEMs way of performing WEM analysis is based on using experience they have developed over decades and I see no obvious obstacles with modelling the entire engine with solid elements other than the computational time. On the other hand, the computational power has increased over the years. If smart geometrical simplifications (which would also have been done when generating a shell model) and a reasonable element size is used, then I do not see more problems with such an approach compared to the current approach when building new WEM. Although, to still save computational time and have the solid representation of selected areas of components, a hybrid version of elements could be used. For instance, the lugs and the fan gearbox could be represented by solid elements and the casings could be represented by shell elements.

12 References

1. Reimers, R., *WEM_DP_v2 - Whole Engine Mechanical Modeling (confidential)*. 2014.
2. Raja, V., *Sub-Modelling of a Jet Engine Component and Creation of Stiffness Interval Based on Cast Dimensional Variations*, in *Management and Engineering*. 2011, Linköpings Universitet
3. NASA. *Turbofan Engine*. 2015 May 5 2015 [cited 2019 February 5]; Available from: https://www.grc.nasa.gov/www/k-12/airplane/aturbf.html.
4. Royce, R., *The Jet Engine*. 2005, London: Rolls-Royce plc.
5. NASA. *How does a jet engine work?* 2014 June 12 2014 [cited 2019 February 27]; Available from: https://www.grc.nasa.gov/www/k-12/UEET/StudentSite/engines.html.
6. Thulin, O., *On the Analysis of Energy Efficient Aircraft Engines*, in *Department of Mechanics and Maritime Sciences*. 2017, Chalmers University of Technology.
7. Airlinerwatch. *This is how the Boeing 797 will look*. 2018 [cited 2019 March 14]; Available from: https://airlinerwatch.com/this-is-how-the-boeing-797-will-look-like/.
8. Ausick, P. *Is This Boeing's Middle-of-the-Market Airplane?* 2016.
9. Avellan, R., *GKN RM200 Engine Concept Design & Performance (confidential)*. 2017.
10. EASA. *Type Certificate Data Sheets*. 2019; Available from: https://www.easa.europa.eu/document-library/type-certificates.
11. Ellbrant, L. and M. Jacobsson, *Notional engine / Notional type design (confidential)*. 2018.
12. Linke-Diesinger, A., *Systems of Commercial Turbofan Engines*. 2008: Springer-Verlag Berlin Heidelberg.
13. Peery and David, *AIRCRAFT STRUCTURES*. 2011, New York: Dover Publications.
14. Petit, O., *Lecture 12 - Chapter 8*, in *Gas turbine technology - MTF171*. 2018, Mechanics and Maritime Sciences Chalmers University of Technology
15. Skybrary. *Federal Aviation Administration (FAA)*. 2016 [cited 2019 March 6]; Available from: https://www.skybrary.aero/index.php/Federal_Aviation_Administration_(FAA).
16. Sjunnesson, et al., *Post mortem analysis report for composite component after fan blade out test (confidential).* 2009.
17. Boström, A., *Rigid body Dynamics*. 2016.
18. Lehto, A., *Implementation of manoeuvre loads for fatigue life assessment of the front frame in the RM12 engine (confidential)*. 2015.
19. Brain, M. *How Gyroscopes Work*. 2000.
20. Brandy, C. *Turbofan Engine Malfunction Recognition and Response*. 1999 [cited 2019 March 12]; Available from: http://www.b737.org.uk/enginemalfunctions.htm
21. Bettebghoe, D., et al., *Bi-objective optimization of pylon-engine-nacelle assembly: weight vs. tip clearance criterion*. 2013.
22. Yu, P., et al., *Dynamic modeling and vibration characteristic analysis of the aero-engine dual-rotor system with Fan blade out* 2017.

23. Engineering, A. *Altair HyperMesh Overview*. 2019 [cited 2019 February 28]; Description of HyperMesh]. Available from: https://altairhyperworks.com/product/hypermesh.
24. Engineering, A. *Altair OptiStruct Overview*. 2019 [cited 2019 March 10]; Description of OptiStruct]. Available from: https://altairhyperworks.com/product/OptiStruct.
25. Engineering, A. *Altair HyperView Overview*. 2019 [cited 2019 March]; 5]. Available from: https://altairhyperworks.com/product/hyperview
26. Engineering, A. *RFORCE*. 2017 [cited 2019 May 15]; Available from: https://altairhyperworks.com/hwhelp/Altair/2017/help/os/topics/solvers/rforce_bulk_r.htm.
27. Holmgren, M., *Subcomponent analysis and load breakdown in jet engine structures*, in *Management and Engineering*. 2011, Linköpings Universitet

Appendix

i. Centre line load transfer

Each load, force and moment, that act on a point, i, can be replaced by an equivalent load at a different point, C, with distance $\boldsymbol{r}_i$ from point i.

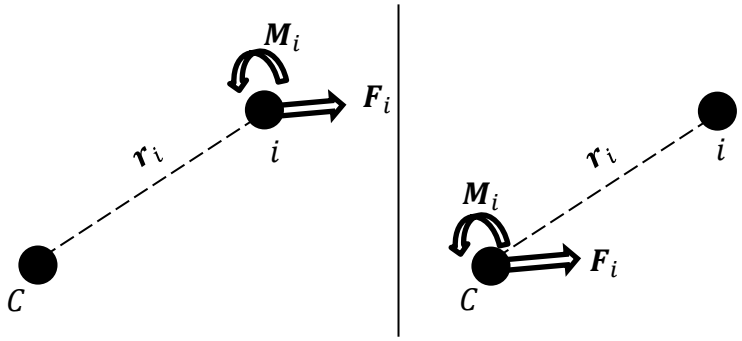

Figure 56: Load transfer from point i to point C.

At circular cross-sections, e.g. the flanges at the SCF, all circumference points will be transferred to the centre point. The forces and moments on the centre point becomes:

$$\boldsymbol{M}_{centre\ node} = \sum_i^N \boldsymbol{r}_i \times \boldsymbol{F}_i + \boldsymbol{M}_i \quad 12$$

$$\boldsymbol{F}_{centre\ node} = \sum_i^N \boldsymbol{F}_i \quad 13$$

where $\boldsymbol{M}_{centre\ node}$ is the equivalent moment at the centre point of the cross-section, $\boldsymbol{F}_{centre\ node}$ is the equivalent force at the centre point of the cross-section. N denotes the number of circumference points, $\boldsymbol{r_i}$ is the distance from the centre point to the point that circumference the cross-section, where index $i = 1,2,3, \dots, N$, $\boldsymbol{F}_i$ denotes the force at point i and $\boldsymbol{M}_i$ denotes the moment at point [27].

ii. Materials in the Notional Engine

The material properties of the CFRP laminate is based on confidential data. In the fiber direction, the Young's modulus is a slightly lower than the Young's modulus of the titanium alloy. In the cross-fiber direction, the Young's modulus is about one third of the Young's modulus in the fiber direction. The density of the CFRP is less than half the density of the titanium alloy.

Table 5: Material data of metals in the Notional Engine.

Material	Young's modulus (E) [GPa]	Poisson's ratio (υ) [-]	Shear modulus (G) [GPa]	Density (ρ) (kg/m^3)	Source
Titanium alloy	114	**0.3**	43.8	4420	A1
Nickel alloy	200	0.29	77.5	8221	A2
Steel alloy	200	**0.3**	76.9	7800	A3
TiAl	153.7	**0.3**	59.1	3900	A4

Where Poisson's ratio has not been indicated, Poisson's ratio is assumed to be equal to 0.3, bold numbers in Table 5.

Table 6: Sources materials in the Notional Engine.

A1	AZO Materials (2019). "Titanium Alloys" from https://www.azom.com/article.aspx?ArticleID=1547
A2	Special Metals Corporation (2007) "INCONEL Alloy". Publication Number SMC-045
A3	ASM Aerospace Specification Metals Inc (2019) "AISI E9310 Steel, annealed at 845°C (1550°F)." from http://asm.matweb.com/search/SpecificMaterial.asp?bassnum=M931AU
A4	A. Brotzu, F. Felli, F. Marra, D. Pilone & G. Pulci (2018) Mechanical properties of a TiAl-based alloy at room and high temperatures, Materials Science and Technology, 34:15, 1847-1853, DOI: 10.1080/02670836.2018.1491931

iii. Estimated Displacement of the Fan Blade in the Sanity Check

Simple hand calculations were used to estimation the right order of magnitude of the tip displacement of the fan blade. In the hand calculations, the fan blade was assumed to behave like a rod, with constant cross-sectional area A, in tension. The fan blade is assumed to be positioned a distance r_0 from the rotational centre and have a length L extending in the radial direction, see Figure 57. The stress, σ, in the fan blade can be calculated as:

$$\sigma = E \cdot \varepsilon = E \cdot \frac{du}{dr}, \qquad 14$$

where E is Young's modulus of the material in the fan blade and $\varepsilon = du/dr$ is the strain of the fan blade.

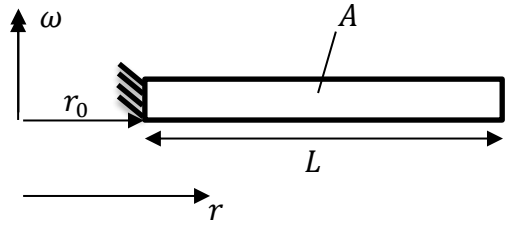

Figure 57: Simplified figure of the fan blade.

The stress in the fan blade can be rewritten as the cross-sectional force, N, on the fan blade divided by the cross-sectional area, A, of the fan blade:

$$\sigma = N/A, \qquad 15$$

The displacement at the tip of the fan blade is investigated by studying the force equilibrium at the cross-section farthest away from the fan blade, see Figure 58.

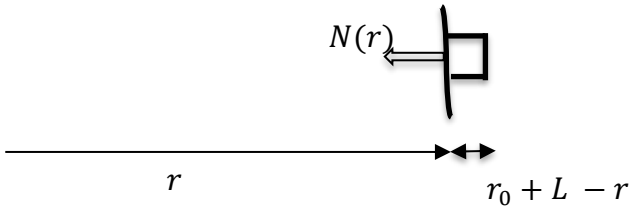

Figure 58: Studying the cross-section farthest away from the fan blade.

Force equilibrium at an arbitrary cross-section at the simplified fan blade gives:

$$-N(r) + \int_r^{L+r_0} dF_R(r) = 0 \qquad 16$$

where F_R is the force caused by the rotation of the fan blade and varies with the distance r from the rotational centre. F_R can be rewritten as

$$dF_R = \omega^2 \cdot r \cdot dm, \qquad 17$$

where ω is the rotational speed of the fan blade and m is the mass of the fan blade.

Inserting Equation 17 into Equation 16 gives:

$$N(r) = \int_r^{L+r_0} \omega^2 r \underbrace{\rho A dr}_{=dm} = \rho A \omega^2 \left[\frac{r^2}{2}\right]_r^{L+r_0} = \frac{\rho A \omega^2}{2}((L+r_0)^2 - r^2) \qquad 18$$

where the mass has been rewritten as $m = \rho A dr$.

Inserting Equation 18 into Equation 15 gives:

$$\sigma(r) = \frac{\rho \omega^2}{2}((L+r_0)^2 - r^2) \rightarrow \frac{du}{dr} = \frac{\rho \omega^2}{2E}((L+r_0)^2 - r^2) \qquad 19$$

Integration gives:

$$u(r) = \frac{\rho\omega^2}{2E}\left((L + r_0)^2 r - \frac{r^3}{3} + C_1\right) \quad 20$$

where C_1 is an integration constant, which will be solved using boundary condition. For the sanity check, the fan blade is assumed to be fixed at the edge closest to the rotational centre, see Figure 57, which gives zero displacement at this inner edge, i.e. $u(r_0) = 0$. C_1 is obtained by solving $u(r_0) = 0$ from Equation 20 and becomes:

$$C_1 = -L^2 r_0 - 2Lr_0^2 - \frac{2r_0^3}{3} \quad 21$$

Inserting C_1 into Equation 20 gives:

$$u(r) = \frac{\rho\omega^2}{2E}\left((L + r_0)^2 r - \frac{r^3}{3} - L^2 r_0 - 2Lr_0^2 - \frac{2r_0^3}{3}\right) \quad 22$$

The displacement at the tip of the fan blade, i.e. the cross-section of the fan blade that is located farthest from the rotational centre becomes:

$$u(L + r_0) = \frac{\rho\omega^2}{2E}\left(\frac{2(L+r_0)^3}{3} - L^2 r_0 - 2Lr_0^2 - \frac{2r_0^3}{3}\right) \quad 23$$

iv. Estimated Force of the Fan Blade in the Sanity Check

The magnitude of the distributed force at the tip of the fan blade, denoted with F_{tip}, that occurs due to the rotation of the fan blade is estimated as the maximum normal force that occurs in the simplified fan blade. This force was used to evaluate if the rotational force implemented RFORCE load gave reasonable results. The normal force, $N(r)$, is determined as:

$$N(r) = \sigma(r) \cdot A(r) = E \cdot \varepsilon(r) \cdot A(r) = E \cdot \frac{du}{dr} \cdot A(r) \qquad 24$$

where $A(r)$ is constant over the entire simplified blade and du/dr is inserted from Equation 19. $N(r)$ is thus obtained as:

$$N(r) = EA \cdot \frac{\rho\omega^2}{2E}((L + r_0)^2 - r^2) \qquad 25$$

The maximum normal force at the blade occurs at the hub of the fan blade, i.e. at $r = r_0$ and becomes:

$$F_{tip} = N_{max} = A \cdot \frac{\rho\omega^2}{2}(L^2 + 2Lr_0) \qquad 26$$

By inserting the variables of the fan blade described in Section 5.3, the estimated magnitude of the force becomes $250kN$, denoted F_{tip}. The direction of the estimated force can be seen in Figure 59.

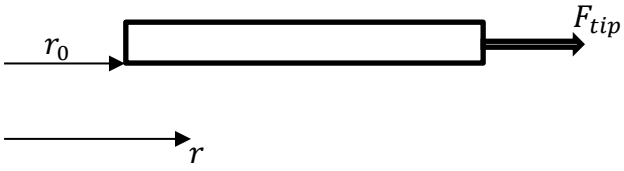

Figure 59: Direction of the estimated force at the tip of the fan blade.

The magnitude of the density was altered so that the total mass of the simplified blade matched the masses of the shell and the solid meshed fan blade. This resulted in different values of the applied load at the different meshed models, i.e. different applied loads on the shell model with constant thickness, the shell model with updated thickness and the solid model.